

FIGURE 4: CAI expression in cell lines. (a) Immunofluorescence detection of CAI in normal prostate epithelial cells and prostate cancer cells. The cells were fixed for 1 h, permeabilized, and stained with antibodies to detect CAI. Alexa Fluor 488- or Alexa Fluor 568-phalloidin was used to visualize normal prostate epithelial cells (upper panels) and prostate cancer cells of 22Rv1 (lower panels). (b) Western blot analysis of media conditioned by the normal prostate epithelial cells and prostate cancer cells probed using a CAI antibody. C3b- α was used as a loading control.

whose PSA levels were within this gray zone were investigated further. Selected cases were as follows: prostate cancer ($n = 30$), BPH ($n = 10$), prostatitis ($n = 2$), and healthy controls ($n = 9$). ROC curves for PSA alone and PSA plus CAI were generated for prostate cancer patients relative to the other cases as described in Materials and Methods (Figure 3(c)). AUCs were 0.763 and 0.694, respectively, for PSA plus CAI and PSA alone in the gray zone. PSA levels had a great discriminatory result with an AUC of 0.939 for all cases. However, PSA levels in the gray zone did not provide sufficient discriminatory power when considered alone. This indicates that CAI levels could improve the PSA assay.

3.4. Subcellular Localization and Secretion of CAI. The subcellular localization of CAI was investigated by immunofluorescence microscopy. CAI was hardly detected in the normal prostate epithelial cells. In comparison to actin as a cytoskeletal marker (red, Figure 4(a), b and e), immunofluorescence

staining with anti-CAI (green, Figure 4(a), a and d) was observed in the cytoplasm of prostate cancer cells (merged, Figure 4(a), f). CAI was clearly detected in media harvested from 22Rv1 cells (Figure 4(b)).

3.5. The Staining of Human Prostate Cancer Cells. CAI was expressed in every case of prostate cancer. Cancer cells from patients with high plasma CAI concentrations tended to have stronger CAI staining than normal prostatic glands (Figure 5).

4. Discussion

We took advantage of our originally developed label-free proteomic technique (2DICAL) [16] to discover a better biomarkers for prostate cancer diagnosis. We identified that CAI peptide fragments were detected at higher levels in plasma samples from prostate cancer patients than in plasma

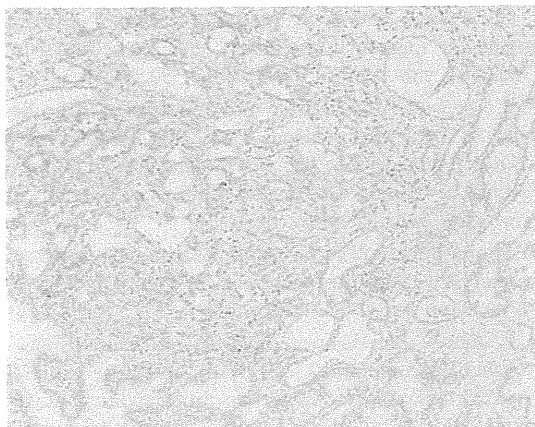


FIGURE 5: Immunohistochemical staining of CAI. CAI was strongly stained at prostate cancer (magnification $\times 100$).

samples from healthy controls. The 2DICAL results were confirmed by Western blot analysis and ELISA using numerous plasma samples including those from patients with urological diseases other than prostate cancer. We found that the combination of CAI and PSA assays has a potential for improving the specificity of PSA assay especially for PSA levels in the gray zone. These initial results suggest that it is reasonable to vigorously pursue CAI as a potentially valuable new biomarker for prostate cancer.

The PSA assay has largely improved the detection of prostate cancer, but only approximately 25% of patients with PSA levels in the gray zone indeed have prostate cancer [19]. Despite the development of several variations of the PSA assay such as free PSA, PSA velocity, or PSA density, these methods do not substantially outperform analysis of total PSA and are not more specific [19, 20]. The reason is because healthy males are known to have PSA levels in the gray zone. Therefore, improved prostate cancer markers such as CAI are eagerly awaited to overcome these problems and enhance diagnostic specificity and sensitivity.

CAI is a zinc metalloenzyme that catalyzes the reversible hydration of carbon dioxide to bicarbonate. Sixteen CA isoforms exist in mammals [21]. Some of them are cytosolic (CAI, CAII, CAIII, CAVII, and CAXIII) catalyzing the hydration of CO_2 to H^+ and HCO_3^- , and subsequently, exporting them from the cell in exchange for Na^+ and Cl^- ions [22]. CAI is a specific marker for the cytoplasm or apical cell membranes of colonic epithelial cells [22, 23] and is related to enterocyte proliferation [24]. CAI is also involved in electroneutral NaCl reabsorption and short chain fatty acid uptake [22]. The biological functions of CAs are of great interest, but CA family members are also being studied as drug targets for treating several diseases such as glaucoma, cancer, obesity, and infections [25].

To the best of our knowledge this is the first report to consider a correlation between CAI blood levels and prostate cancer. To verify the upregulation of plasma CAI in prostate cancer, we investigated the cell biology of prostate cancer using immunofluorescent staining to elucidate its subcellular localization, and Western blotting of culture media to

determine if CAI was secreted. We demonstrated increased CAI production and secretion in prostate cancer cell lines. Stronger staining of CAI was observed in prostate cancer cells from patients with high plasma CAI concentrations compared to that in normal prostate glands. However, to clarify the mechanism of the plasma concentration change of CAI, further investigations will be needed considering the secretion mechanism of CAI from prostate cancer cells.

Our present proteome research is new in that we found increased plasma CAI levels in prostate cancer patients. Furthermore, it indicates the possibility that CAI was produced and secreted by prostate cancer cell lines. This study may lead to clinically using CAI as a new prostate cancer marker and the combination of PSA and CAI may have great advantages for diagnosing prostate cancer in patients with gray-zone PSA levels.

Conflict of Interests

The authors have no conflict of interests.

Authors' Contribution

M. Takakura and A. Yokomizo contributed equally to the study.

Acknowledgments

The authors thank Ms. Ayako Ikarashi, Ms. Tomoko Umaki, and Ms. Yuka Nakamura for their technical assistance. Funding was provided by the Program for Promotion of Fundamental Studies in Health Sciences conducted by the National Institute of Biomedical Innovation of Japan, the Third-Term Comprehensive Control Research for Cancer and Research on Biological Markers for New Drug Development conducted by the Ministry of Health and Labor of Japan. These sponsors had no role in the design of the study, collection of the data, analysis and interpretation of the data, decision to submit the paper for publication, or writing of the paper.

References

- [1] A. Jemal, R. Siegel, E. Ward, Y. Hao, J. Xu, and M. J. Thun, "Cancer statistics, 2009," *CA—A Cancer Journal for Clinicians*, vol. 59, no. 4, pp. 225–249, 2009.
- [2] W. J. Catalona, D. S. Smith, T. L. Ratliff, and J. W. Basler, "Detection of organ-confined prostate cancer is increased through prostate-specific antigen-based screening," *JAMA*, vol. 270, no. 8, pp. 948–954, 1993.
- [3] J. Pannek and A. W. Partin, "Prostate-specific antigen: what's new in 1997," *Oncology*, vol. 11, no. 9, pp. 1273–1278, 1997.
- [4] S. Loeb, S. N. Gashti, and W. J. Catalona, "Exclusion of inflammation in the differential diagnosis of an elevated prostate-specific antigen (PSA)," *Urologic Oncology*, vol. 27, no. 1, pp. 64–66, 2009.
- [5] W. J. Catalona, J. P. Richie, F. R. Ahmann et al., "Comparison of digital rectal examination and serum prostate specific antigen in the early detection of prostate cancer: Results of a

- multicenter clinical trial of 6,630 men,” *Journal of Urology*, vol. 151, no. 5, pp. 1283–1290, 1994.
- [6] W. J. Catalona, D. S. Smith, and D. K. Ornstein, “Prostate cancer detection in men with serum PSA concentrations of 2.6 to 4.0 ng/mL and benign prostate examination: Enhancement of specificity with free PSA measurements,” *JAMA*, vol. 277, no. 18, pp. 1452–1455, 1997.
- [7] A. Magklara, A. Scorilas, W. J. Catalona, and E. P. Diamandis, “The combination of human glandular Kallikrein and free prostrate-specific antigen (PSA) enhances discrimination between prostate cancer and benign prostatic hyperplasia in patients with moderately increased total PSA,” *Clinical Chemistry*, vol. 45, no. 11, pp. 1960–1966, 1999.
- [8] J. Cervera Deval, F. J. Morales Olaya, J. Jornet Fayos, and M. González Añón, “Diagnostic value of the second prostate biopsies in males of risk. Study stratified by value of PSA,” *Actas Urológicas Españolas*, vol. 28, no. 9, pp. 666–671, 2004.
- [9] M. Raber, V. Scattoni, A. Salonia, P. Consonni, and P. Rigatti, “Repeated ultrasound-guided transrectal prostate biopsy in patients with negative histologic test,” *Archivio Italiano di Urologia, Andrologia*, vol. 72, no. 4, pp. 197–199, 2000.
- [10] M. Ono, M. Shitashige, K. Honda et al., “Label-free quantitative proteomics using large peptide data sets generated by nanoflow liquid chromatography and mass spectrometry,” *Molecular and Cellular Proteomics*, vol. 5, no. 7, pp. 1338–1347, 2006.
- [11] A. Negishi, M. Ono, Y. Handa et al., “Large-scale quantitative clinical proteomics by label-free liquid chromatography and mass spectrometry,” *Cancer Science*, vol. 100, no. 3, pp. 514–519, 2009.
- [12] M. Ono, J. Matsubara, K. Honda et al., “Prolyl 4-hydroxylation of α -fibrinogen. A novel protein modification revealed by plasma proteomics,” *The Journal of Biological Chemistry*, vol. 284, no. 42, pp. 29041–29049, 2009.
- [13] Y. Murakoshi, K. Honda, S. Sasazuki et al., “Plasma biomarker discovery and validation for colorectal cancer by quantitative shotgun mass spectrometry and protein microarray,” *Cancer Science*, vol. 102, no. 3, pp. 630–638, 2011.
- [14] J. Matsubara, K. Honda, M. Ono et al., “Reduced plasma level of CXC chemokine ligand 7 in patients with pancreatic cancer,” *Cancer Epidemiology Biomarkers and Prevention*, vol. 20, no. 1, pp. 160–171, 2011.
- [15] A. Yokomizo, M. Takakura, Y. Kanai et al., “Use of quantitative shotgun proteomics to identify fibronectin 1 as a potential plasma biomarker for clear cell carcinoma of the kidney,” *Cancer Biomarkers*, vol. 10, no. 3-4, pp. 175–183, 2011.
- [16] M. Ono, M. Kamita, Y. Murakoshi et al., “Biomarker discovery of pancreatic and gastrointestinal cancer by 2DICAL: 2-dimensional image-converted analysis of liquid chromatography and mass spectrometry,” *International Journal of Proteomics*, vol. 2012, Article ID 897412, 10 pages, 2012.
- [17] Y. Tanaka, H. Akiyama, T. Kuroda et al., “A novel approach and protocol for discovering extremely low-abundance proteins in serum,” *Proteomics*, vol. 6, no. 17, pp. 4845–4855, 2006.
- [18] M. Idogawa, T. Yamada, K. Honda, S. Sato, K. Imai, and S. Hirohashi, “Poly(ADP-ribose) polymerase-1 is a component of the oncogenic T-cell factor-4/beta;-catenin complex,” *Gastroenterology*, vol. 128, no. 7, pp. 1919–1936, 2005.
- [19] H. Lilja, D. Ulmert, and A. J. Vickers, “Prostate-specific antigen and prostate cancer: Prediction, detection and monitoring,” *Nature Reviews Cancer*, vol. 8, no. 4, pp. 268–278, 2008.
- [20] S. Loeb and W. J. Catalona, “What to do with an abnormal PSA test,” *Oncologist*, vol. 13, no. 3, pp. 299–305, 2008.
- [21] C. T. Supuran and A. Scozzafava, “Carbonic anhydrases as targets for medicinal chemistry,” *Bioorganic and Medicinal Chemistry*, vol. 15, no. 13, pp. 4336–4350, 2007.
- [22] E. R. Swenson, “Distribution and functions of carbonic anhydrase in the gastrointestinal tract,” in *Carbonic Anhydrases: Cellular Physiology and Molecular Genetics*, S. J. Dodgson, R. E. Tashian, G. Gros, and N. D. Carter, Eds., pp. 265–287, Plenum Press, New York, NY, USA, 1991.
- [23] G. Lonnerholm and P. Wistrand, “Carbonic anhydrase in the human fetal gastrointestinal tract,” *Biology of the Neonate*, vol. 44, no. 3, pp. 166–176, 1983.
- [24] I. B. Renes, M. Verburg, D. J. P. M. Van Nispen et al., “Epithelial proliferation, cell death, and gene expression in experimental colitis: Alterations in carbonic anhydrase I, mucin MUC2, and trefoil factor 3 expression,” *International Journal of Colorectal Disease*, vol. 17, no. 5, pp. 317–326, 2002.
- [25] C. T. Supuran, “Carbonic anhydrase inhibition/activation: Trip of a scientist around the world in the search of novel chemotypes and drug targets,” *Current Pharmaceutical Design*, vol. 16, no. 29, pp. 3233–3245, 2010.

Large-scale Identification of Endogenous Secretory Peptides Using Electron Transfer Dissociation Mass Spectrometry*[§]

Kazuki Sasaki[‡], Tsukasa Osaki[‡], and Naoto Minamino[‡]

Mass spectrometry-based unbiased analysis of the full complement of secretory peptides is expected to facilitate the identification of unknown biologically active peptides. However, tandem MS sequencing of endogenous peptides in their native form has proven difficult because they show size heterogeneity and contain multiple internal basic residues, the characteristics not found in peptide fragments produced by *in vitro* digestion. Endogenous peptides remain largely unexplored by electron transfer dissociation (ETD), despite its widespread use in bottom-up proteomics. We used ETD, in comparison to collision induced dissociation (CID), to identify endogenous peptides derived from secretory granules of a human endocrine cell line. For mass accuracy, both MS and tandem MS were analyzed on an Orbitrap. CID and ETD, performed in different LC-MS runs, resulted in the identification of 795 and 569 unique peptides (ranging from 1000 to 15000 Da), respectively, with an overlap of 397. Peptides larger than 3000 Da accounted for 54% in CID and 46% in ETD identifications. Although numerically outperformed by CID, ETD provided more extensive fragmentation, leading to the identification of peptides that are not reached by CID. This advantage was demonstrated in identifying a new antimicrobial peptide from neurosecretory protein VGF (non-acronymic), VGF[554–577]-NH₂, or in differentiating nearly isobaric peptides (mass difference less than 2 ppm) that arise from alternatively spliced exons of the gastrin-releasing peptide gene. CID and ETD complemented each other to add to our knowledge of the proteolytic processing sites of proteins implicated in the regulated secretory pathway. An advantage of the use of both fragmentation methods was also noted in localization of phosphorylation sites. These findings point to the utility of ETD mass spectrometry in the global study of endogenous peptides, or peptidomics. *Molecular & Cellular Proteomics* 12: 10.1074/mcp.M112.017400, 700–709, 2013.

Biologically active peptides, commonly known as peptide hormones and antimicrobial peptides, belong to a defined set

From the [‡]Department of Molecular Pharmacology, National Cerebral and Cardiovascular Center Research Institute, Suita, Osaka 565–8565, Japan

Received January 24, 2012, and in revised form, October 10, 2012
Published, MCP Papers in Press, December 18, 2012, DOI 10.1074/mcp.M112.017400

of endogenous peptides that gain specialized functions not ascribed to original precursor proteins. For a precursor protein to generate such peptides, it must undergo specific cleavages and in some cases needs to be modified at specific sites (1). This limited cleavage, or proteolytic processing, represents an important cellular mechanism by which molecular diversity of proteins is increased at the post-translational level. In the postgenome era, it is being recognized that localization of processing sites in secretory proteins facilitates the identification of biologically active peptides. A standard approach to determining such sites is to use a panel of antibodies directed against different regions of a target protein (2). However, it is practically impossible to prepare antibodies that can thoroughly cover potential processing products arising from the precursor. Alternatively, mass spectrometry-assisted unbiased analysis of endogenous peptides may be a major step toward elucidating proteolytic processing (3).

In neurons and endocrine cells, a majority of biologically active peptides are released via the regulated secretory pathway. They are stored in secretory granules and await secretion until the cells receive an exocytotic stimulus. Owing to their compartmentalization, secretory peptides can be noninvasively recovered in culture supernatant. We have shown that a data set of endogenous peptide sequences that are collected by this procedure is applicable to infer processing sites, as well as to identify bona fide processing products (4). Rather than being digested, every endogenous peptide should be analyzed in its native form to understand how the peptide is generated and subsequently degraded. However, it remains a challenge to identify endogenous peptides because of size heterogeneity (ranging from 3 aa to 100 aa). For example, thyrotropin-releasing hormone is a small 3-aa peptide, human adrenomedullin occurs as a 52-aa peptide, and a 98-aa N-terminal propeptide from the atrial natriuretic peptide precursor is found in the circulation. Unlike digested protein fragments used in bottom-up proteomics, C termini of these endogenous peptides are not restricted to specific residues. Furthermore, proteolytic processing leads to the production of peptides containing multiple internal basic residues, for which collision induced dissociation (CID)¹ shows limited performance (5).

¹ The abbreviations used are: CID, collision induced dissociation; CgB, chromogranin B; ETD, electron transfer dissociation; GRP, gastrin-releasing peptide; PC, prohormone convertase.

A solution to address this issue in endogenous peptide sequencing might be the use of electron transfer dissociation (ETD) tandem mass spectrometry, which has been shown to provide a more complete series of fragment ions and hence a more confident sequence identification, along with the ability to leave labile post-translational modifications intact (6–10). The benefit of ETD in bottom-up proteomics has been increasingly documented, whereas endogenous peptides remain largely unexplored by ETD, despite the expectation that ETD would improve sequencing for larger peptides. In the few studies on endogenous peptides (11, 12), ETD did not cover large peptides exceeding 5000 Da. Because we have used CID to facilitate the discovery of previously unknown biologically active peptides (3, 13, 14), we were interested to see if ETD would be helpful to identify endogenous peptides that have escaped identification by CID. Here we conducted a large-scale identification of endogenous secretory peptides, ranging from 1000 to 15000 Da, using CID and ETD. We describe the merits of using ETD, in connection with CID, in peptidomics studies. The most significant finding is the identification of a previously unknown peptide, VGF[554–577]-NH₂, which was sequenced solely by ETD. This peptide was found to have antimicrobial activity.

EXPERIMENTAL PROCEDURES

Sample Preparation—The human islet cell line QGP-1 (~1 × 10⁷ cells) (15) was stimulated with 10 μM carbachol plus 50 mM potassium chloride in serum-free Hank's balanced solution. Five minutes after stimulation, the medium was harvested to recover released peptides. The supernatant was quickly subjected to solid extraction as previously described (4). The eluate was separated by gel filtration high-performance liquid chromatography (HPLC) to five fractions containing peptides in the approximate *M_r* range 1000 to 15000.

Liquid Chromatography-Tandem Mass Spectrometry—All data were acquired on an LTQ Orbitrap XL instrument equipped with ETD (Thermo Fisher Scientific, San Jose, CA). A nanoFrontier HPLC system (Hitachi, Japan) was connected to the mass spectrometer for liquid chromatography-tandem mass spectrometry (LC-MS/MS). About 300 to 500 ng of the peptide mixture was loaded onto a trap column (C18, 75 μm × 100 mm) and separated on a MonoSpray C18 tip (GL Sciences) using a 60-min gradient from 10 to 50% acetonitrile in 0.1% formic acid at a flow rate of 200 nL/min. A protonated ion of polycyclodimethylsiloxane with *m/z* 445.120025 was used for internal calibration throughout. The mass spectrometer alternated between a full FT-MS scan (*m/z* 400–1500) and subsequent MS/MS scans. Scans were all recorded in the Orbitrap with a resolution of 100,000 at *m/z* 400. CID and ETD were performed on separate LC-MS runs. Cations were isolated with an isolation window of 5 *m/z* units and provided on a dynamic exclusion list for 2400 s after selected for at least two MS/MS scans. Singly charged precursors were excluded. Monoisotopic selection was disabled with an exclusion window setting to 1 Da. The four most intense ions were chosen for CID fragmentation. Automatic gain control was used to accumulate sufficient fragment ions (MS/MS target value, 2E5; maximum injection time, 1000 ms). For ETD, the two most intense precursor ions were subjected to MS/MS with an ETD activation time of 90 ms for doubly charged ions. Charge state-dependent activation time was applied. The ETD activation time was optimized for enhancing peptide identification by testing four different periods of time (70, 90, 150, and 200 ms) and also consistent with a previous report conducted on endog-

enous peptides using an ETD-enabled LTQ-XL (10). Supplemental activation was used for all MS/MS scans (16). ETD spectra were acquired using one microscan per spectrum. Automatic gain control was also used (MS/MS target value, 5E5; fluoranthene, 1E6; maximum fill time, 1500 ms). Samples were not subjected to reductive alkylation. However, an aliquot of the sample was reductively alkylated using dithiothreitol and iodoacetamide to identify peptides derived from chromogranin B (CgB), whose N-terminal region contains two cysteine residues forming a disulfide bond.

Data Analysis and Peptide Identification—Peak picking, deisotoping, and deconvolution of MS/MS spectra were conducted using Mascot Distiller (version 2.2.3) with the default parameters for Orbitrap. Peak lists were searched against NCBI nr human (14,987,464 sequences; 5,132,678,026 residues, as of August 13, 2011) using Mascot (version 2.2.3) with no enzyme specification. Pyroglutamination, C-terminal amidation, N-terminal acetylation, and methionine oxidation were simultaneously allowed as variable modifications. Data were searched with a precursor mass tolerance of 5 ppm and product ion mass tolerance of 50 mmu. Peptides were considered identified with a Mascot expect value of less than 0.05. The false discovery rate for peptide matches above Mascot identity threshold using a decoy database search was 0% in all cases. The highest scored MS/MS spectrum was used to report the score of the unique peptide in supplemental Table S2. The percent fragmentation was calculated as reported (8), with N-terminal proline cleavage also included as a possible fragmentation channel. In Mascot notation, the even-electron c ion corresponds to the b ion plus NH₃. Mascot does not try to match radical c-1 ions, which are usually much weaker. The charged radical z+1 ion is the y ion minus NH₂. Hence, the most abundant z-type ions observed in ETD are radical z+1 and even-electron z+2. For calculating percent fragmentation, z-type ions were counted only once if both z+1 and z+2 ions were assigned by Mascot for a given N-Cα bond.

Peptide Synthesis—Peptides were synthesized by the solid phase method (Sigma Genosys, Japan) using Fmoc (N-(9-fluorenyl) methoxycarbonyl) strategy, purified by reverse phase HPLC, and verified for correct synthesis by MS and amino acid analysis. Peptide purity was confirmed on separate HPLC systems.

Antibody Preparation and Mass Spectrometric Characterization of Immunoreactivity—CysteinyI C-terminal 13-residue peptide of human VGF[554–577]-NH₂ (CHYHHALPPSRHYP-NH₂) was conjugated with maleimide-activated keyhole limpet hemocyanin (Thermo Fisher Scientific). Rabbits were immunized every 3 weeks with the conjugate emulsified with Freund's complete adjuvant. Antiserum (#529–6) was characterized in a radioimmunoassay system (dilution 1/900,000, IC50 = 8 fmol/tube), which completely crossreacted with VGF[554–577]-NH₂ but showed no crossreactivity with VGF[554–578] or VGF[554–583]. Furthermore, ten C-terminally amidated peptides (human calcitonin gene-related peptide[23–37]-NH₂, pig neuromedin U-8, neurokinin A, vasopressin, human adrenomedullin[22–52]-NH₂, human calcitonin, pig peptide histidine isoleucine, ovine corticotropin-releasing factor, proadrenomedullin N-terminal 20-amino acid peptide, calcitonin receptor stimulating peptide-1[24–28]-NH₂) showed less than 0.01% cross reactivity up to 100 pmol/tube. Cell culture supernatant was immunoprecipitated with the antibody and analyzed on a surface-enhanced laser desorption and ionization mass spectrometer as described (17).

Antibacterial and Antifungal Activity Assay—Each test peptide (up to 10 μM) was assessed with the target microbes *Enterococcus hirae* (*E. hirae*), *Micrococcus luteus* (*M. luteus*), *Staphylococcus aureus* (*S. aureus*) 209P, *S. saprophyticus* KD, *Escherichia coli* (*E. coli*) B, *E. coli* K12, *E. coli* kp, and *Pichia pastoris* (*P. pastoris*) GS115 using AlamarBlue™ (BioSource International, Camarillo, CA) (14, 18). The optimal growth temperature was 30 °C for *M. luteus*, *S. saprophyticus* KD and

Utility of ETD in Peptidomics

P. pastoris GS115 and 37 °C for the other microbes. After growth in 3% tryptosoy broth (Eiken Chemical, Tokyo, Japan) for 16 h with shaking at each optimal temperature, cells were washed twice with 10 mM phosphate buffer, pH 7.0, and diluted to 8×10^5 colony-forming units/ml in the same buffer. Twenty-five microliters of bacterial suspension were mixed with an equal volume of sample in the absence or presence of peptides, and incubated for 1 h. After incubation, 200 μ l of 3% tryptosoy broth containing 10% alamarBlue™ was added to the reaction mixture and further incubated for the period of time shown in parentheses: *E. hirae*, *S. aureus* 209P and *E. coli* B (4 h), *E. coli* K12 and *E. coli* kp (6 h), *M. luteus* (7 h), *S. saprophyticus* KD (7.5 h), and *P. pastoris* GS115 (20 h). Aliquots containing all assay reagents without microbes were used as blank. After incubation, the reactions were monitored by absorbance at 569 and 600 nm. Molar extinction coefficients of OD₅₆₉ and OD₆₀₀ in the oxidative condition are 80586 and 117216. Viability (%) was expressed using the following formula: viability (%) = $(117216 \times OD_{569} - 80586 \times OD_{600} \text{ with peptide}) / (117216 \times OD_{569} - 80586 \times OD_{600} \text{ without peptide}) \times 100$. The classical colony formation assay was performed on *M. luteus*, *E. coli* K12 and *P. pastoris* GS115 as described (18). Cathelicidin and β -defensin-2 (Peptide Institute, Osaka, Japan) were used as control.

RESULTS

We studied a complex mixture of peptides secreted by cultured human endocrine cells that received an exocytotic stimulus. The culture supernatant was harvested 5 mins after stimulation and separated by gel filtration HPLC to five fractions containing peptides in the approximate M_r range 1000 to 15000. LC-MS/MS was performed in duplicate for each fraction on an LTQ-Orbitrap equipped with ETD. For comparison, the same sample was independently analyzed by CID in duplicate runs. Both MS and MS/MS scans were recorded with Orbitrap to ensure sequencing of highly charged peptide ions ($z > 4$). The high mass accuracy and resolution enabled by Orbitrap allowed searching the human NCBI nr database with no enzyme specification and acquire significant data, and despite this broad search space the false discovery rate for peptide matches above the identity threshold using a Mascot automatic decoy database search was 0%.

In a total of 20 runs, 2311 and 1733 peptides (including redundant identifications) were identified by CID and ETD, respectively. In Table I, these peptides were sorted according to precursor charge states and fragmentation methods. No peptide was identified using ETD of doubly charged ions although supplemental activation was applied. Aside from this, there was no apparent difference in charge distribution between CID and ETD. More than two-thirds of the peptides were quadruply or more highly charged (69% for CID and 76% for ETD). This charge distribution is skewed, relative to that commonly observed with digested peptides used in bottom-up proteomics, most of which are doubly or triply charged ions. To assess the degree of peptide dissociation, we calculated the percent fragmentation values, defined by Coon *et al.* (8) as the number of observed fragment ions (b- and y-type ions for CID and c- and z-type ions for ETD), for a peptide sequence, divided by the total theoretically possible number of fragment ions. The percent fragmentation was

TABLE I
Total peptide identifications sorted by fragmentation method and precursor charge state

Precursor charge state	CID	ETD
+2	252	0
+3	454	417
+4	451	449
+5	431	300
+6	398	299
+7	220	146
+8	77	60
+9	14	16
+10	6	15
+11	4	23
+12	3	7
+13	1	0
+14	0	1
Total	2311	1733

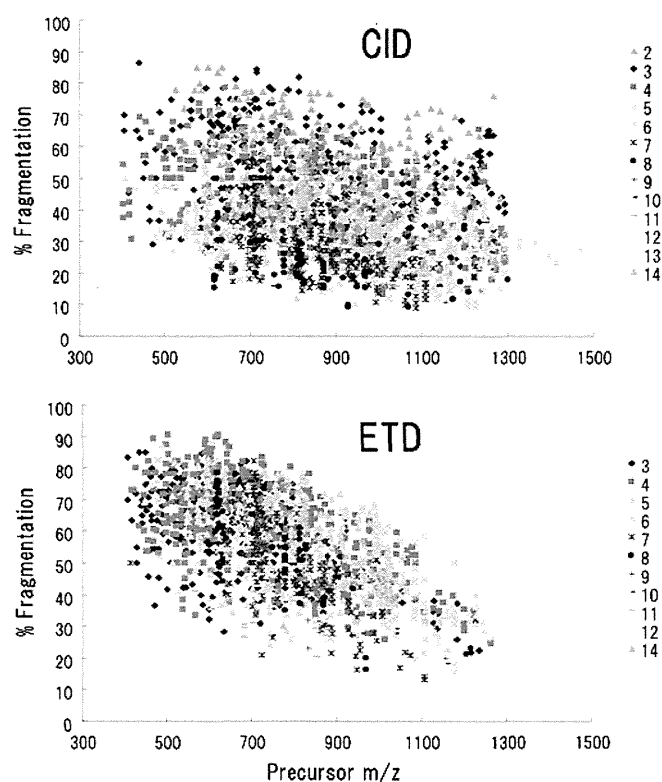


Fig. 1. Percent fragmentation, defined as the number of observed fragment ions divided by the theoretical number of fragment ions, plotted against precursor m/z . Plotted data are from 2311 CID-identified and 1733 ETD-identified peptides.

plotted as a function of m/z values of the identified precursors (Fig. 1, supplemental Table S1). In CID, charge states and precursor m/z values showed little influence on percent fragmentation. Consistent with the previous study (8, 10), ETD percent fragmentation was decreased as precursor ion m/z increases regardless of charge state. Although surpassed by CID in the overall number of identification, ETD provided more extensive fragmentation; nearly 12% of the ETD-identified

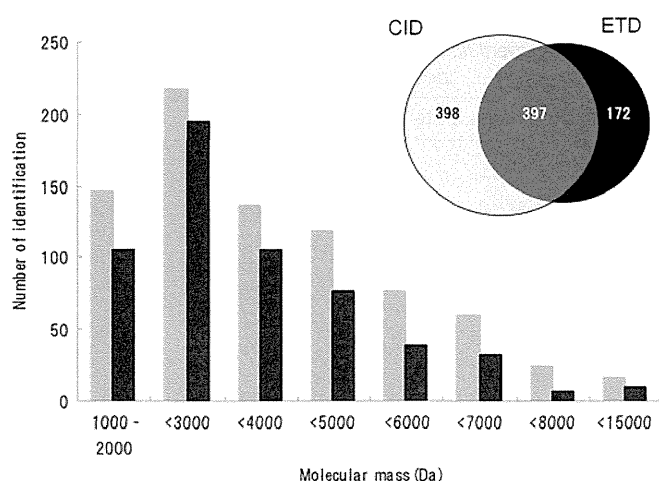


FIG. 2. Mass distribution of CID- and ETD-identified peptides. Only unique peptides were counted. (Inset) Venn diagram illustrating the number of unique peptides identified by CID and ETD.

peptides have percent fragmentation values greater than 75, as compared with 2% of the CID-identified peptides.

After removing redundant identifications caused by either peptide overlaps between two adjacent gel filtration fractions or ionization of the same peptide into different charge states, we concluded that CID and ETD elucidated 795 and 569 unique peptides, respectively, with the overlap being 397 (Fig. 2, supplemental Table S2). Peptides larger than 3000 Da accounted for 54 and 46% in CID and ETD identifications, respectively. Notably, nearly 96% of the peptides arose from secretory precursor proteins. Judged by the number of peptides, our analyte appeared to contain relatively large amounts of VGF and chromogranin B (CgB) (supplemental Table S2). They contain multiple pairs of basic residues, some of which have been described as cleavage sites for processing to biologically active peptides (2, 19).

The identified peptides derived from VGF and CgB were aligned to each precursor sequence and illustrated in Fig. 3. They are shown by gray (CID) and black (ETD) lines and stacked to highlight potential processing sites. Multiple lines of the same length indicate redundant identifications. By inspecting the cleavage sites revealed by these lines, we inferred primary processing sites that involve at least one basic residue (dotted lines, Fig. 3). The VGF sequence was almost completely covered by clusters of peptides sharing N termini or C termini, whereas CgB showed less coverage. No peptide was ascribed to the signal sequence. Previously, a limited number of VGF-derived peptides were reported in peptidomics work on human cerebrospinal fluid using CID (20–22). We conducted a more detailed study by analyzing the culture supernatant from a human endocrine cell line and tissue extracts in normal rat brain and gut (3, 4, 23). In earlier work, several CgB-derived peptides have been isolated from extracts of human pheochromocytoma and neuroendocrine tumors (24–26). The specific processing sites that have been

proposed by those studies are indicated in Fig. 3. Although differences in species and tissue sources should be taken into account, these sites extensively overlap the potential processing sites revealed by the present study.

On close inspection some peptides were identified solely by ETD, an example of which is VGF[554–577]-NH₂ (Fig. 3, supplemental Table S2). This C-terminally amidated peptide underwent extensive fragmentation at every possible N-C α bond except the Pro-Ser (positions 572–573), whereas CID showed poor fragmentation (Fig. 4). The lack of ETD cleavage N-terminal to proline is consistent with the previous work on proline-containing synthetic peptides (7). In triplicate analyses, this peptide, detected as quadruply and pentuply charged ions, had a percent fragmentation of 54 to 61% and 56 to 63%, respectively. It might be noteworthy that N-terminally truncated 13- and 14-residue peptides sharing the C-terminal amide structure were solely identified by CID. Antibody specifically recognizing the amide structure was generated to characterize major peptide forms. Major peptides immunoprecipitated with the antibody from the culture supernatant had the molecular masses corresponding to the theoretical masses of VGF[554–577]-NH₂ and [565–577]-NH₂ (supplemental Fig. S1). Similar results were obtained with the supernatant from the human medullary thyroid carcinoma cell line TT (data not shown). We thus concluded that these two peptides represent major processing products.

The three consecutive arginine residues in VGF[554–577]-NH₂ prompted us to test antimicrobial activity, along with the related peptides (Table II). VGF[554–583], identified in the present study, was tested because it was C-terminally flanked by the dibasic residues that correspond to the N-terminal processing site of VGF[586–615]/AQEE-30 (Fig. 3a). VGF[554–577]-NH₂ showed antimicrobial activity against *M. luteus* and *P. pastoris*, comparable to the established antimicrobial peptides β -defensin-2 and cathelicidin, whereas C-terminally extended VGF[554–578] and [554–583] were less potent. Up to the concentrations tested, VGF[565–577]-NH₂ was not active against any of the test microbes (Table II and Fig. 5). To examine whether VGF[554–577]-NH₂ is bactericidal or just bacteriostatic, we performed a classical colony formation assay. It has been established that the bactericidal peptide concentration revealed by classical colony formation assays and the alamarBlue™ assay shows a good agreement (17). The peptide showed strong antimicrobial activity in the colony assay with IC₅₀ of 1.9 and 1.4 μ M against *M. luteus* and *P. pastoris*, respectively (data not shown), indicating that it is bactericidal.

It remains a challenge to pinpoint a post-translationally modified site among multiple candidate sites in a sequence, because informative fragment ions for unequivocal localization are not always observed in MS/MS spectra. A total of 13 phosphopeptides were identified using CID and ETD without any phosphopeptide enrichment procedure (Table III). As a consequence, five unique modified sites were identified from six peptides, of which Ser130 of CgB identified in 4684.98-Da

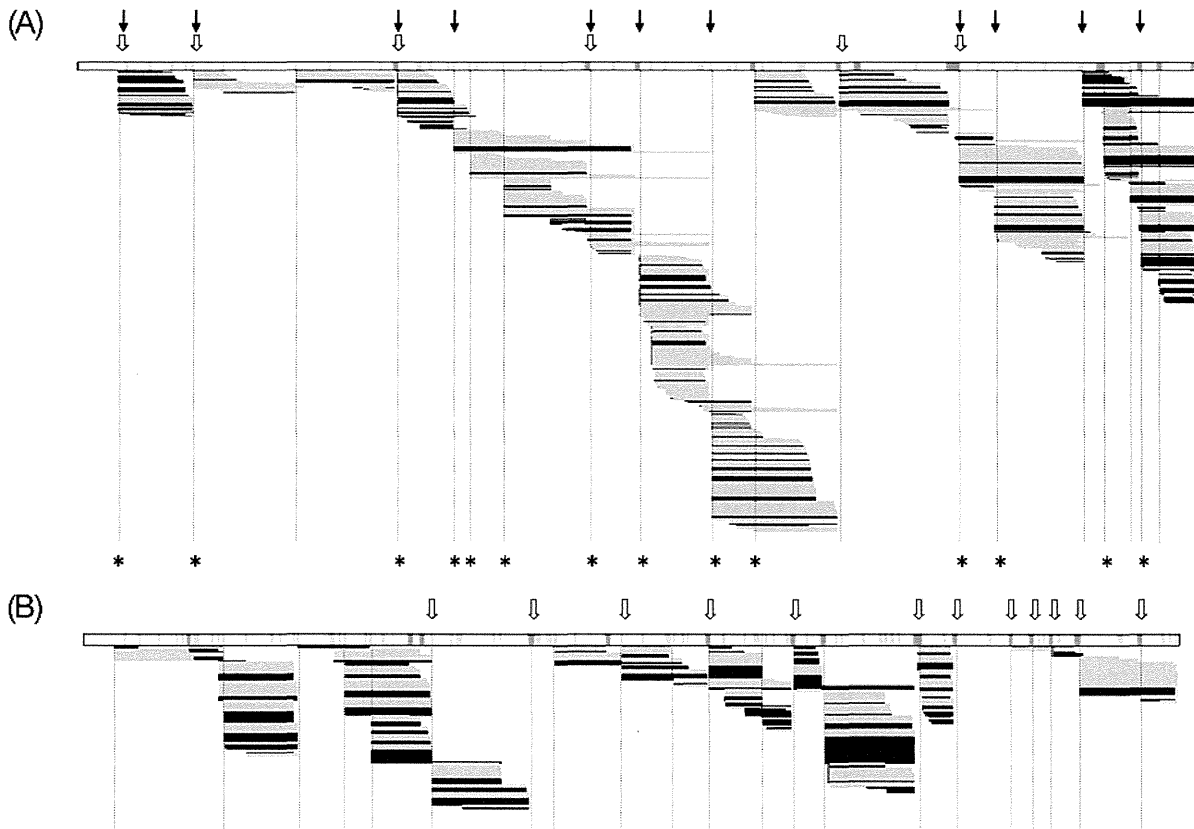


FIG. 3. Identified peptides derived from VGF (GI: 17136078) (A) and CgB/secretogranin-1 (GI: 36439) (B). Gray lines, CID-identified peptides; black lines, ETD-identified peptides. Red boxes, pyroglutamination; yellow boxes, C-terminal amidation. Note that the maps include redundant identifications, excluding oxidized methionine-containing peptides. Processing sites proposed by previous studies in human VGF (20–22) and human CgB (2, 24–26) are indicated by open arrows above the precursor sequence. In (A), arrows indicate processing sites identified in rat brain studies (13, 23). Asterisks indicate processing sites proposed in our previous peptidomics study of a different human endocrine cell line (3). Processing sites inferred from the present study are shown in vertical dotted lines. Magenta bars, consecutive basic residues. Pale magenta bars, single basic residues.

and 5067.25-Da peptides and Ser64 of the calcitonin precursor identified in 6297.01-Da peptide have not previously been described. Two phosphorylation sites in CgB, Ser335 of 6109.65-Da and Ser617 of 7049.27-Da peptides, were previously described (27), but represent fortuitous cases where CID, rather than ETD, allowed successful identification. Ser405 of the CgB 3730.65-Da peptide, previously determined as a phosphorylation site through conventional techniques (26), was confidently reconfirmed by ETD (supplemental Fig. S2). We got evidence that the VGF- and secretogranin II-derived peptides are phosphorylated, but failed to localize modified sites.

Except for phosphopeptides, the unique peptide sequences listed in supplemental Table S2 excluded any peptide for which the second-ranked sequence also has a Mascot expectation value of 0.05 or lower. However, we encountered one exceptional case; CID of a positively charged ion (+6) with m/z 808.24 resulted in the identification of the amidated peptide from gastrin-releasing peptide (GRP) isoform 1 preproprotein[95–139]-NH₂ (calculated monoisotopic mass 4843.377), with a Mascot score of 120 (expt. 3.5E-08). Ranked second was the peptide from GRP isoform 2

preproprotein[95–138] (calculated monoisotopic mass 4843.369), with a score of 96 close to the top (expt. 9.1E-06). The two peptides share N-terminal 27 residues but have alternatively spliced C-terminal halves (Fig. 6). The fragment ions produced by CID were preferentially observed the N-terminal region so that distinguishing these two possibilities was difficult. In ETD, the first rank was the peptide from GRP isoform 1 (score 289, expt. 4.5E-25) and the second was from GRP isoform 2 (score 82, expt. 0.00022). Although both hits still exceed a stringent threshold (expectation < 0.001, rather than a default value of 0.05), we concluded that this peptide arises from the isoform 1 because of the extensive matching to theoretical ions (Fig. 6). It might be worth mentioning that GRP isoform 1 preproprotein[54–139]-NH₂ (calculated monoisotopic mass 9514.789), which is N-terminally adjacent to the amidation motif of neuromedin C, was also identified by CID (supplemental Fig. S2).

DISCUSSION

We have shown that mass spectrometric analysis of endogenous secretory peptides provides a basis for identifying bi-

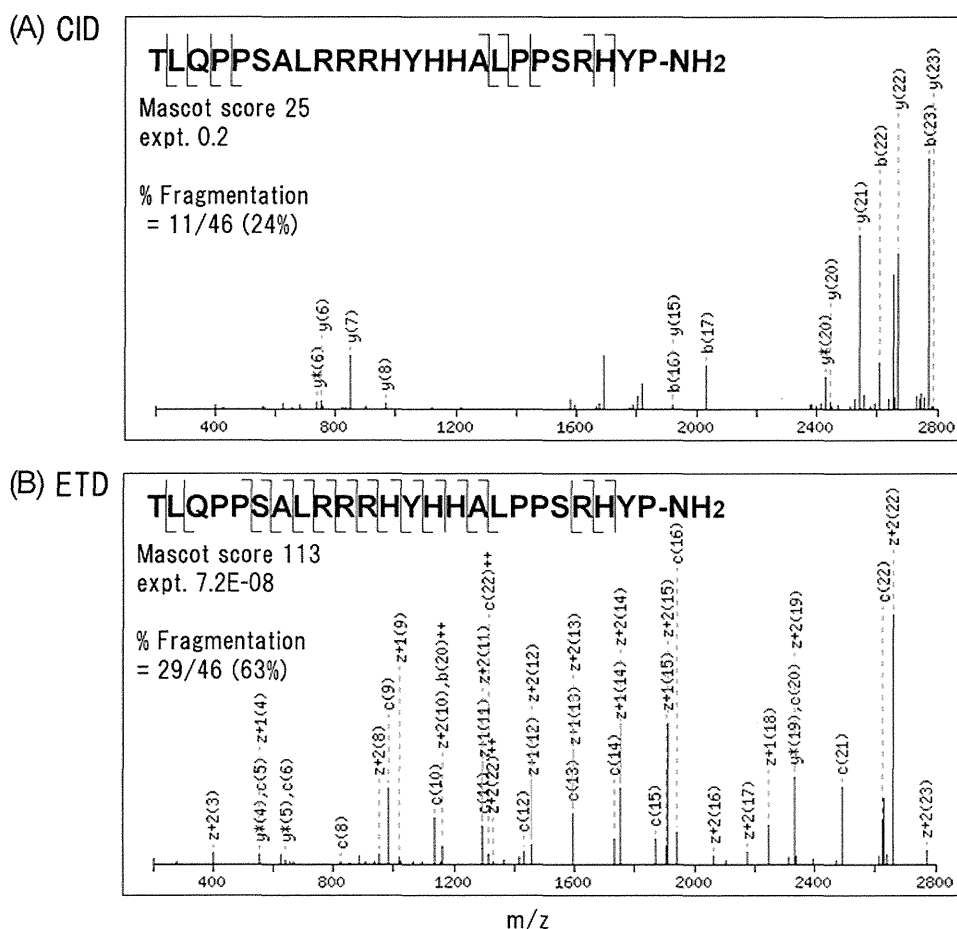


FIG. 4. Deconvoluted CID (A) and ETD (B) MS/MS spectra of pentuply charged VGF[554–577]-NH₂.

TABLE II
Antimicrobial activity assayed by the alamarBlue method. NI, no inhibition up to 10 μ M

Peptide	<i>M. luteus</i>	<i>E. coli</i> K12	<i>P. pastoris</i> GS115
VGF[554–577]-NH ₂	1.8	NI	4.5
VGF[554–578]	5.6	NI	NI
VGF[554–583]	5.8	NI	NI
VGF[565–577]-NH ₂	NI	NI	NI
β -Defensin-2	0.7	5.6	2.6
Cathelicidin	1.3	0.6	3.1

ologically active peptides (3, 13, 14). In the present study, our immediate interest is to uncover endogenous peptides that escape identification by CID. Endogenous peptides remain largely unexplored by ETD or electron capture dissociation, whose performance for such peptides has not been thoroughly characterized. ETD was used on a low-end ion trap mass spectrometer to characterize venom peptides extracted from a marine snail (28), resulting in a fraction of small peptides (less than 3000 Da) being sequenced. Shen *et al.* recently used the same instrumentation as ours to improve endogenous peptide identification, but identified peptides

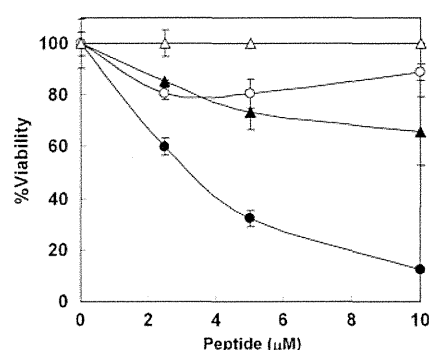


FIG. 5. Antimicrobial activity of VGF[554–577]-NH₂ and related peptides against *P. pastoris* GS115. VGF[554–577]-NH₂ (closed circle), [554–578] (closed triangle), [565–577]-NH₂ (open circle) and [554–578] (open triangle) were assayed using alamarBlue.

came from doubly to quadruply charged ions in most cases (12). Thus little is known at present about the ability of ETD to dissociate endogenous peptides with higher charge states, despite the occurrence of large endogenous peptides (>5000 Da) in larger amounts than previously thought.

It has been generally accepted that ETD is more effective than CID for sequencing highly charged precursors or larger peptides in bottom-up proteomics (6–9). However, our pep-

TABLE III

Endogenous phosphopeptide identification

Mascot scores of first to third hits (columns 6 to 8) are accompanied by expectation values shown in parentheses. N-term, N-terminal flanking amino acid ("Signal" indicates that the peptide is flanked by signal sequence); C-term, C-terminal flanking amino acid. Identified phosphorylation sites are marked in bold and underlined. In the last column, the asterisk indicates that either of the two N-terminal serine residues is phosphorylated but not uniquely determined. CT, calcitonin; SgII, secretogranin II.

Method	Precursor	m/z (obsd.)	z	M_r (calc.) (Da)	1st Hit	2nd Hit	3rd Hit	N-term	Sequence	C-term	Reference
Unequivocal localization											
CID	CgB	1175.887	6	7049.271	94 (1.9E-05)	49 (0.6)	28 (77)	K	S AEFDPFDYDSEEPVSTHQEAENEKDRADQTVLTEDEK KELENLAAMDLELQKIAEKFSQR-NH ₂	G	(27)
CID	CgB	1222.937	5	6109.646	60 (3.6E-02)	9 (4.5E+03)	6 (8.0E+03)	R	A SEEEPEYGEIIGYPGVQAPEDLEWERYRGRGS EEYRAPRPQSEESWDEE	D	(27)
CID	CgB	845.549	6	5067.250	82 (2.2E-04)	45 (1)	35 (10)	R	LLRDPADASEAHESSSRGEAGAPGEEDIQGPTKA DTEKWAEGGGHSRE	R	
ETD	CgB	938.004	5	4684.981	109 (2.9E-07)	60 (0.023)	39 (3.1)	R	DPADASEAHESSSRGEAGAPGEEDIQGPTKADTEK WAEGGGHSRE	R	
ETD	CgB	747.137	5	3730.647	136 (6.5E-10)	12 (1.6E+03)	4 (8.7E+03)	R	NYPSELDKMAHGYGEESSEERGLEPGKGRHH	R	(26)
ETD	CT	1260.409	5	6297.006	65 (0.016)	42 (3.1)	41 (3.8)	Signal	APFRSALESSPADPATLSEDEARLLLALVQDYVQM KASELEQEEREGSSLDSPRS	K	
Ambiguous localization											
ETD	CgB	845.006	5	4219.991	139 (4.3E-10)	138 (4.4E-10)	67 (0.0063)	R	GEDSSEEKHLEEPGETQNAFLNERKQASAIKKEELVA	R	(27)*
CID	SgII	1138.077	7	7959.485	78 (0.00075)	71 (0.003)	71 (0.003)	R	ERMDEEQKLYTDDDDIYKANNIAYEDVVGGEDWNP VEEKIESQTQEEVRDSKENIEKNEQINDEM	K	
CID	SgII	1280.066	6	7674.341	103 (2.5E-06)	95 (1.5E-05)	95 (1.5E-05)	R	MDEEQKLYTDDDDIYKANNIAYEDVVGGEDWNPV EEKIESQTQEEVRDSKENIEKNEQINDEM	K	
ETD	SgII	1030.079	5	5145.363	70 (0.0038)	70 (0.0038)	63 (0.018)	R	ALEYIENLRQQAHKKESSPDYNPYQGVSVPLQQKE NGDESHLPE	R	
CID	VGF	1117.343	6	6698.003	168 (7.8E-13)	168 (7.8E-13)	168 (7.8E-13)	R	SQEETPGHRRKEAEGTEEGGEEEDDEEMDPQTIDSL IELSTKLHLPADDVVSIIIEVEE	K	
ETD	VGF	807.197	5	4030.954	115 (9.2E-08)	105 (8.1E-07)	0.5 (2.5E+04)	Signal	APPGRPEAQPPPLSSEHKPEVAGDAVPGPKDGS APEVRGA	R	
ETD	VGF	937.707	4	3746.794	91 (2.3E-05)	77 (0.0005)	6 (7.0E+03)	Signal	APPGRPEAQPPPLSSEHKPEVAGDAVPGPKDGSAPEV	R	

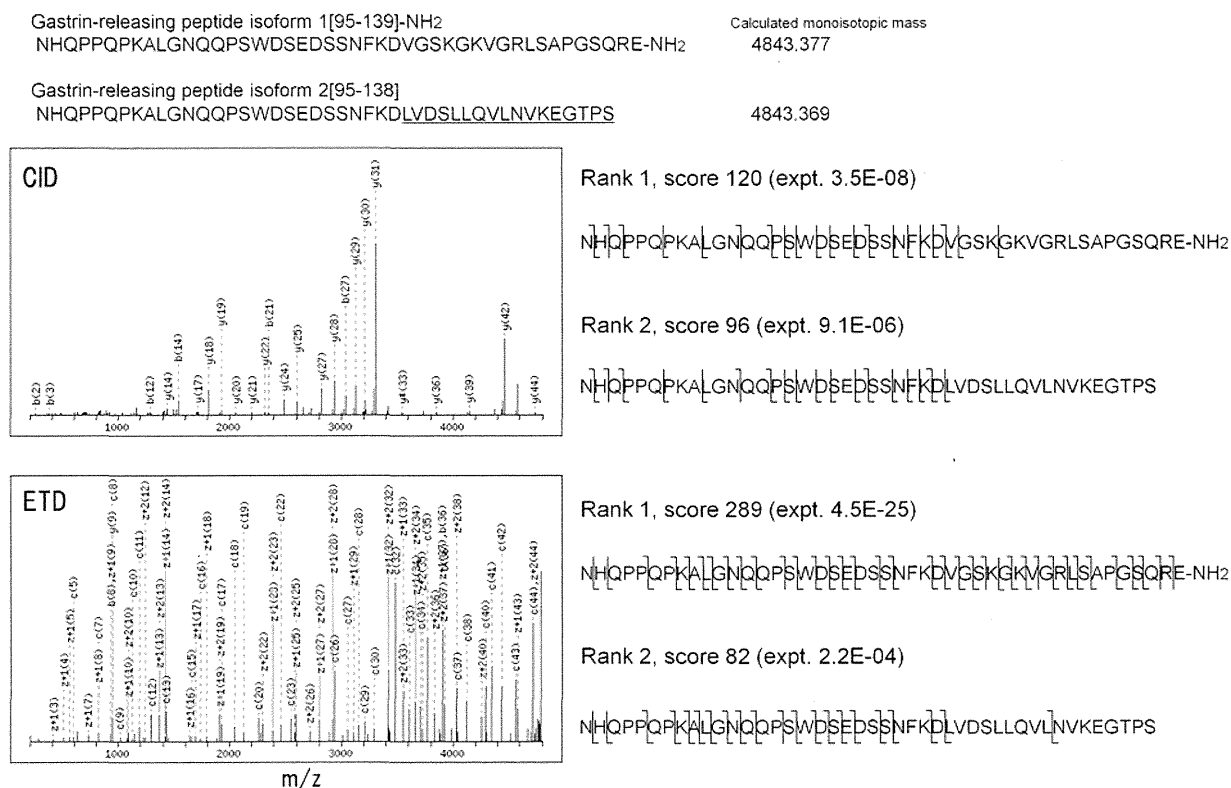


FIG. 6. **Deconvoluted CID and ETD MS/MS spectra of sextuply charged m/z 808.24.** Alternatively spliced exons of the GRP gene produce two nearly isobaric peptides. Residues different from the top peptide are underlined in the lower peptide. Note that the second best matches for both fragmentations are below a Mascot expect value of 0.05, but that ETD showed a wider difference between the best and second best matches because of extensive fragmentations across the sequence.

tidomic data indicate that CID was as potent as ETD in sequencing precursors having charges greater than three, with their proportions being 69% for CID and 76% for ETD. Furthermore, CID appears to be superior to ETD in total identification; 795 peptides for CID *versus* 569 peptides for ETD. For peptides larger than 7000 Da, CID uncovered a larger number of peptides than ETD (39 for CID and 15 for ETD). Good *et al.* reported that a linear decrease in percent fragmentation as a function of increasing precursor m/z was noted for ETD, with few peptides having precursor m/z values exceeding 850 identified (8). We also observed a similar but less remarkable decline; in our study peptides identified with precursors greater than m/z 850 still accounted for 30% (507 of 1733) in the total ETD identification. This difference in ETD performance may be partly explained by the fact that most of our secretome components have more internal basic residues than *in vitro*-digested proteins. The current limitation in ETD was particularly noted with precursors having higher m/z values ($m/z > 1300$). Supplemental Fig. S3 shows CID and ETD of two pentuply charged precursors with m/z 1324.6 and 1411.7. They were unequivocally identified by CID as 6618.0-Da VGF-derived peptide and 7053.5-Da N-terminal propeptide of the somatostatin precursor, whereas the corresponding ETD spectra were so dominated by

charge reduced species that no significant match was obtained.

We provided the most comprehensive data about VGF and CgB processing. Both fragmentation methods complemented each other to highlight potential cleavage sites more clearly than that provided by either alone. Because they represent major components in neuronal secretory vesicles and several peptides identified here have also been described as neuropeptides (2, 19, 29), our findings will contribute to neuropeptide profiling in neuropeptidomics. The VGF processing sites predicted here are consistent with the antibody-assisted biochemical characterization of major processing products in rat brain (23). For instance, the 7400 Da peptide (also known as TLQP-62 (29)) in the rat study corresponds to human VGF[554–615] (calculated monoisotopic mass 7498.98), and rat 15166 Da and 7047 Da peptides recognized by NERP-2 antibody correspond to human VGF[208–347]-NH₂ and VGF[281–347]-NH₂ (calculated monoisotopic mass 14832.74 and 7108.77), respectively.

CgB-derived peptides have been isolated from human pituitary and pheochromocytoma tissues without reference to biological activity or immunoreactivity (2, 24–26), including CgB[217–275], [293–323], [326–385], [334–385], [388–437], [440–513](GAWK), [518–537], [575–585](PE-11), [588–597],

[600–613](BAM-1745), and [617–676](CCB). All the peptides but CgB[326–385] were identified in the present study. Flanked by either pairs or groups of basic amino acids, they are considered specific processing products. Despite the presence of potential cleavage sites across the sequence, no peptide has been described in the literature for the N-terminal 216-amino acid region. Our data revealed that the precursor undergoes extensive processing across the entire sequence, including previously reported processing sites (Fig. 3B). The reason for the lack of peptide identification for positions 540–572 remains to be elucidated.

Some peptides were solely identified by ETD, including CgB-derived GAWK of 8788.13 Da (24) and VGF[554–577]-NH₂. This C-terminally amidated peptide had escaped MS/MS identification because of poor CID fragmentation in our previous peptidomic survey (3). In the present study, ETD was able to provide an almost complete series of ions to ensure confident identification; it has five proline residues, where cleavage N-terminal to proline is missing in ETD (7). Considering this proline effect, the peptide has 18 theoretically cleavable bonds rather than 23. As shown in Fig. 4, 17 of the 18 bonds were cleaved. Of note, related N-terminally truncated peptides were not revealed by ETD, demonstrating the advantage of using different dissociation techniques. The ability of ETD to cleave peptide backbone across the entire sequence was also demonstrated in distinguishing between the peptides derived from two different isoforms of the neuropeptide GRP gene, again reflecting the merits of ETD in peptidomics. The high mass accuracy and resolution attained by Orbitrap enables discrimination between z+1 and z+2 ions, ensuring in some cases that z+2 matches in Mascot are not 13C isotope peaks of z+1 matches.

In rat brain, TLQP-62/rat VGF[556–617] was originally described as a major peptide recognized by antibody against the protein C terminus (29). The N-terminal 556Thr is 554Thr in human VGF. An appreciable number of the peptides starting with 554Thr were revealed by ETD, including VGF[554–577]-NH₂, [554–583] and [554–615] (Fig. 3A). Given the sequence identity between human and rat, the cleavage site (PR↓TLQP) may represent a major processing site also in human. These peptides have not been described in peptidomic reports of VGF-derived peptides (3, 20–22). On the other hand, the C-terminal cleavage site has recently been described through MS/MS identification of VGF[565–577]-NH₂ (3). Because 574RHYPGR579 agrees with the consensus motif for prohormone convertase (PC) 1/3 or 2 ((K/R)-(X)_n-(K/R)↓, where *n* = 0, 2, 4, or 6 and X is any amino acid other than Cys) (30) and is nested by a canonical amidation signal of 578GR579, generation of the amidated peptides can be explained by the general rule of proteolytic processing in the regulated secretory pathway (30). This is also supported by the fact that the complete set of enzymes involved in C-terminal amidation, PC1/3 or 2, carboxypeptidase E, and pepti-

dylglycine α-amidating monooxygenase were expressed by the cell line used (not shown).

VGF[554–577]-NH₂ showed antimicrobial activity against *M. luteus* and *P. pastoris*, comparable to major antimicrobial peptides β-defensin-2 and cathelicidin. The N-terminal 11 residues are considered essential for activity, because N-terminally truncated VGF[565–577]-NH₂ was inactive. In addition, the decreased activity observed with the two C-terminally extended peptides suggests that the C-terminal amide structure is important as well. It is known that amidated C termini, rather than common carboxyl termini, help to enhance electrostatic interactions between the peptide and a target bacterial membrane (31). This may also be the case with this peptide. The amidation motif is not found in rodent VGF sequences, but shared by primates (supplemental Fig. S1C), suggesting that the peptide is assigned some biological role unique to primates.

We were able to identify phosphopeptides of intermediate size (3500 to 8000 Da). Two phosphorylation sites, not described in the literature, were unequivocally localized. Of note, all but one (6109.65-Da peptide) of the 13 peptides were both N-terminally and C-terminally flanked by previously reported signal sequence cleavage sites or PC1/3 or PC2 consensus sites, strongly suggesting that they are bona fide secretory phosphopeptides. Although not explored, phosphorylated peptides quickly released via exocytosis may have some functional roles in the nervous and endocrine systems. Because larger peptides lead to less confident identification of modification sites than smaller peptides, ETD parameters should be further optimized. We conclude that CID and ETD complement each other to advance our understanding of endogenous peptides, which has received limited attention in the proteomics community.

Acknowledgments—We thank Professor Toshifumi Takao (Osaka University, Japan) for his advice on peptide identification by LC-MS/MS. We also thank Junko Kimata, Makoto Takahata, and Morihiko Yoshida (Thermo Fisher Scientific, Japan) for their technical assistance in ETD studies, Itaru Usami and John Cottrell (Matrix Science, United Kingdom) for their help with Mascot, and Masako Matsubara (National Cerebral and Cardiovascular Center) for data analysis.

* This study was supported in part by the Intramural Research Fund of the National Cerebral and Cardiovascular Center, a Health Labor Sciences Research Grant from The Ministry of Health Labor and Welfare, and a Grant-in-Aid for Scientific Research from the Japan Society for the Promotion of Science.

☐ This article contains supplemental Tables S1 and S2 and Figs. S1 to S3.

¶ Present address, Department of Molecular Patho-Biochemistry and Patho-Biology of Hematology and Circulation, Yamagata University School of Medicine, 2-2-2 Iida-Nishi, Yamagata, Yamagata 990-9585, Japan.

§ To whom correspondence should be addressed: Department of Molecular Pharmacology, National Cerebral and Cardiovascular Center Research Institute, 5-7-1 Fujishirodai, Suita, Osaka 565-8565, Japan. Tel.: +81 6 6833 5004; Fax: +81 6 6835 5349; E-mail: kasaki@ri.nccvc.go.jp.

REFERENCES

- Fricker, L. D. (2005) Neuropeptide-processing enzymes: applications for drug discovery. *AAPS J.* **7**, E449–455
- Stridsberg, M., Eriksson, B., Oberg, K., and Janson, E. T. (2005) A panel of 13 region-specific radioimmunoassays for measurements of human chromogranin B. *Regul. Pept.* **125**, 193–199
- Sasaki, K., Takahashi, N., Satoh, M., Yamasaki, M., and Minamino, N. (2010) A peptidomics strategy for discovering endogenous bioactive peptides. *J. Proteome Res.* **9**, 5047–5052
- Sasaki, K., Satomi, Y., Takao, T., and Minamino, N. (2009) Snapshot peptidomics of the regulated secretory pathway. *Mol. Cell. Proteomics* **8**, 1638–1647
- Tabb, D. L., Huang, Y., Wysocki, V. H., and Yates, J. R., 3rd (2004) Influence of basic residue content on fragmentation ion peak intensities in low-energy collision-induced dissociation spectra of peptides. *Anal. Chem.* **76**, 1243–1248
- Syka, J. E., Coon, J. J., Schroeder, M. J., Shabanowitz, J., and Hunt, D. F. (2004) Peptide and protein sequence analysis by electron transfer dissociation mass spectrometry. *Proc. Natl. Acad. Sci. U.S.A.* **101**, 9528–9533
- Mikesh, L. M., Ueberheide, B., Chi, A., Coon, J. J., Syka, J. E., Shabanowitz, J., and Hunt, D. F. (2006) The utility of ETD mass spectrometry in proteomic analysis. *Biochim Biophys Acta.* **1764**, 1811–1822
- Good, D. M., Wirtala, M., McAlister, G. C., and Coon, J. J. (2007) Performance characteristic of electron transfer dissociation mass spectrometry. *Mol. Cell. Proteomics* **24**, 517–533
- Molina, H., Horn, D. M., Tang, N., Mathivanan, S., and Pandey, A. (2007) Global proteomic profiling of phosphopeptides using electron transfer dissociation tandem mass spectrometry. *Proc. Natl. Acad. Sci. U.S.A.* **104**, 2199–2204
- Good, D. M., and Coon, J. J. (2009) Mass spectrometric analysis of body fluids for biomarker discovery. *Methods Mol. Biol.* **566**, 277–291
- Hui, L., Cunningham, R., Zhang, Z., Cao, W., Jia, C., and Li, L. (2011) Discovery and characterization of the Crustacean hyperglycemic hormone precursor related peptides (CPRP) and orckinin neuropeptides in the sinus glands of the blue crab *Callinectes sapidus* using multiple tandem mass spectrometry techniques. *J. Proteome Res.* **10**, 4219–4229
- Shen, Y., Tolić, N., Purvine, S. O., and Smith, R. D. (2012) Improving collision induced dissociation (CID), high energy collision dissociation (HCD), and electron transfer dissociation (ETD) Fourier transform MS/MS degradome-peptidome identifications using high accuracy mass information. *J. Proteome Res.* **11**, 668–677
- Yamaguchi, H., Sasaki, K., Satomi, Y., Shimbara, T., Kageyama, H., Mondal, M. S., Toshinai, K., Date, Y., González, L. J., Shioda, S., Takao, T., Nakazato, M., and Minamino, N. (2007) Peptidomic identification and biological validation of neuroendocrine regulatory peptide-1 and -2. *J. Biol. Chem.* **282**, 26354–26360
- Osaki, T., Sasaki, K., and Minamino, N. (2011) Peptidomics-based discovery of an antimicrobial peptide derived from insulin-like growth factor-binding protein 5. *J. Proteome Res.* **10**, 1870–1880
- Iguchi, H., Hayashi, I., and Kono, A. (1990) A somatostatin-secreting cell line established from a human pancreatic islet cell carcinoma (somatostatinoma): release experiment and immunohistochemical study. *Cancer Res.* **50**, 3691–3693
- Swaney, D. L., McAlister, G. C., Wirtala, M., Schwartz, J. C., Syka, J. E., and Coon, J. J. (2007) Supplemental activation method for high-efficiency electron-transfer dissociation of doubly protonated peptide precursors. *Anal. Chem.* **79**, 477–485
- Sasaki, K., Sato, K., Akiyama, Y., Yanagihara, K., Oka, M., and Yamaguchi, K. (2002) Peptidomics-based approach reveals the secretion of the 29-residue COOH-terminal fragment of the putative tumor suppressor protein DMBT1 from pancreatic adenocarcinoma cell lines. *Cancer Res.* **62**, 4894–4898
- Osaki, T., Omotezako, M., Nagayama, R., Hirata, M., Iwanaga, S., Kasahara, J., Hattori, J., Ito, I., Sugiyama, H., and Kawabata, S. (1999) Horseshoe crab hemocyte-derived antimicrobial polypeptides, tachystatins, with sequence similarity to spider neurotoxins. *J. Biol. Chem.* **274**, 26172–26178
- Levi, A., Ferri, G. L., Watson, E., Possenti, R., and Salton, S. R. (2004) Processing, distribution, and function of VGF, a neuronal and endocrine peptide precursor. *Cell Mol. Neurobiol.* **24**, 517–533
- Selle, H., Lamerz, J., Buerger, K., Dessauer, A., Hager, K., Hampel, H., Karl, J., Kellmann, M., Lannfelt, L., Louhija, J., Riepe, M., Rollingner, W., Tuman, H., Schrader, M., and Zucht, H. D. (2005) Identification of novel biomarker candidates by differential peptidomics analysis of cerebrospinal fluid in Alzheimer's disease. *Comb. Chem. High Throughput Screen.* **8**, 801–806
- Huang, J. T., Leweke, F. M., Oxley, D., Wang, L., Harris, N., Koethe, D., Gerth, C. W., Nolden, B. M., Gross, S., Schreiber, D., Reed, B., and Bahn, S. (2006) Disease biomarkers in cerebrospinal fluid of patients with first-onset psychosis. *PLoS Med.* **3**, e428
- Zougman, A., Pilch, B., Podtelejnikov, A., Kiehnopf, M., Schnabel, C., Kumar, C., and Mann, M. (2008) Integrated analysis of the cerebrospinal fluid peptidome and proteome. *J. Proteome Res.* **7**, 386–399
- Mishiro-Sato, E., Sasaki, K., Matsuo, T., Kageyama, H., Yamaguchi, H., Date, Y., Matsubara, M., Ishizu, T., Yoshizawa-Kumagaye, K., Satomi, Y., Takao, T., Shioda, S., Nakazato, M., Minamino, N. (2010) Distribution of neuroendocrine regulatory peptide-1 and -2, and proteolytic processing of their precursor VGF protein in the rat. *J. Neurochem.* **114**, 1097–1106
- Benjannet, S., Leduc, R., Lazure, C., Seidah, N. G., Marcinkiewicz, M., and Chrétien, M. (1985) GAWK, a novel human pituitary polypeptide: isolation, immunocytochemical localization and complete amino acid sequence. *Biochem. Biophys. Res. Commun.* **126**, 602–609
- Conlon, J.M., Hamberger, B., and Grimelius, L. (1992) Isolation of peptides arising from the specific posttranslational processing of chromogranin A and chromogranin B from human pheochromocytoma tissue. *Peptides* **13**, 639–644
- Dahma, H., Gourlet, P., Vancermers, A., Vandermeers-Piret, M. C., and Robberecht, P. (2001) Evidence that the chromogranin B fragment 368–418 extracted from a pheochromocytoma is phosphorylated. *Peptides* **22**, 1491–1499
- Beranova-Giorgianni, S., Zhao, Y., Desiderio, D. M., and Giorgianni, F. (2006) Phosphoproteomic analysis of the human pituitary. *Pituitary* **9**, 109–120
- Ueberheide, B. M., Fenyő, D., Alewood, P. F., and Chait, B. T. (2009) Rapid sensitive analysis of cysteine rich peptide venom components. *Proc. Natl. Acad. Sci. U.S.A.* **106**, 6910–6915
- Bartolomucci, A., Possenti, R., Mahata, S. K., Fischer-Colbrie, R., Loh, Y. P., and Salton, S. R. (2011) The Extended Granin Family: Structure, Function, and Biomedical Implications. *Endocr. Rev.* **32**, 755–797
- Cameron, A., Apletalina, E. V., and Lindberg, I. (2002) The enzymology of PC1 and PC2, in *The Enzymes* (Dalby, R. E., and Sigman, D. S., eds) pp. 291–328, Academic Press, New York, NY
- Dos Santos Cabrera, M. P., Arcisio-Miranda, M., Broggio Costa, S. T., Konno, K., Ruggiero, J. R., Procopio, J., and Ruggiero Neto, J. (2008) Study of the mechanism of action of anoplín, a helical antimicrobial decapeptide with ion channel-like activity, and the role of the amidated C-terminus. *J. Pept. Sci.* **14**, 661–669

Direct Immunochemiluminescent Assay for proBNP and Total BNP in Human Plasma proBNP and Total BNP Levels in Normal and Heart Failure

Toshio Nishikimi^{1*}, Hiroyuki Okamoto², Masahiro Nakamura², Naoko Ogawa², Kazukiyo Horii², Kiyoshi Nagata², Yasuaki Nakagawa¹, Hideyuki Kinoshita¹, Chinatsu Yamada¹, Kazuhiro Nakao¹, Takeya Minami¹, Yoshihiro Kuwabara¹, Koichiro Kuwahara¹, Izuru Masuda³, Kenji Kangawa⁴, Naoto Minamino⁵, Kazuwa Nakao¹

1 Department of Medicine and Clinical Science, Kyoto University Graduate School of Medicine, Kyoto, Japan, **2** Diagnostics Division, Shionogi & Co., Ltd, Osaka, Japan, **3** Takeda Hospital Medial Examination Center, Kyoto, Japan, **4** Department of Biochemistry National Cerebral and Cardiovascular Center Research Institute, Osaka, Japan, **5** Department of Molecular Pharmacology, National Cerebral and Cardiovascular Center Research Institute, Osaka, Japan

Abstract

Background: Recent studies have shown that in addition to brain (or B-type) natriuretic peptide (BNP) and the N-terminal proBNP fragment, levels of intact proBNP are also increased in heart failure. Moreover, present BNP immunoassays also measure proBNP, as the anti-BNP antibody cross-reacts with proBNP. It is important to know the exact levels of proBNP in heart failure, because elevation of the low-activity proBNP may be associated with the development of heart failure.

Methodology/Principal Findings: We therefore established a two-step immunochemiluminescent assay for total BNP (BNP+proBNP) and proBNP using monoclonal antibodies and glycosylated proBNP as a standard. The assay enables measurement of plasma total BNP and proBNP within only 7 h, without prior extraction of the plasma. The detection limit was 0.4 pmol/L for a 50- μ l plasma sample. Within-run CVs ranged from 5.2%–8.0% in proBNP assay and from 7.0%–8.4% in total BNP assay, and between-run CVs ranged from 5.3–7.4% in proBNP assay and from 2.9%–9.5% in total BNP assay, respectively. The dilution curves for plasma samples showed good linearity (correlation coefficients=0.998–1.00), and analytical recovery was 90–101%. The mean total BNP and proBNP in plasma from 116 healthy subjects were 1.4 ± 1.2 pM and 1.0 ± 0.7 pM, respectively, and were 80 ± 129 pM and 42 ± 70 pM in 32 heart failure patients. Plasma proBNP levels significantly correlate with age in normal subjects.

Conclusions/Significance: Our immunochemiluminescent assay is sufficiently rapid and precise for routine determination of total BNP and proBNP in human plasma.

Citation: Nishikimi T, Okamoto H, Nakamura M, Ogawa N, Horii K, et al. (2013) Direct Immunochemiluminescent Assay for proBNP and Total BNP in Human Plasma proBNP and Total BNP Levels in Normal and Heart Failure. PLoS ONE 8(1): e53233. doi:10.1371/journal.pone.0053233

Editor: German E. Gonzalez, University of Buenos Aires, Cardiovascular Pathophysiology Institute, Argentina

Received: July 10, 2012; **Accepted:** November 26, 2012; **Published:** January 24, 2013

Copyright: © 2013 Nishikimi et al. This is an open-access article distributed under the terms of the Creative Commons Attribution License, which permits unrestricted use, distribution, and reproduction in any medium, provided the original author and source are credited.

Funding: This study was supported in part by Scientific Research Grants-in-Aid 20590837 and 23591041 from the Ministry of Education, Culture, Sports, Science and Technology of Japan (to T. Nishikimi); a grant (AS 232Z01302F) from the Japan Science and Technology Agency (to T. Nishikimi); a grant from the Suzuken Memorial Foundation (to T. Nishikimi); and the Intramural Research Fund of National Cerebral and Cardiovascular Center of Japan (to N. Minamino). The funders had no role in study design, data collection and analysis, decision to publish, or preparation of the manuscript.

Competing Interests: Hiroyuki Okamoto, Masahiro Nakamura, Naoko Ogawa, Kazukiyo Horii and Kiyoshi Nagata are employed by Shionogi & Co., Ltd. Shionogi Company previously developed the BNP kit and they may develop a new assay kit like a proBNP in the future. There are no further patents, products in development or marketed products to declare. This does not alter the authors' adherence to all the PLOS ONE policies on sharing data and materials.

* E-mail: nishikim@kuhp.kyoto-u.ac.jp

Introduction

Brain (also known as B-type) natriuretic peptide (BNP) has been used as a biomarker of heart failure for more than a decade [1]. Indeed, guidelines for the treatment of heart failure recommend measurement BNP before making a diagnosis [2,3]. During the process by which BNP is secreted from cardiac myocytes, its 108-amino acid precursor, proBNP, is cleaved to form the 32-amino acid peptide BNP and the 76-amino acid peptide N-terminal proBNP fragment (NT-proBNP) [4]. Recent studies have shown that in addition to BNP and the NT-proBNP, levels of uncleaved proBNP are also considerably increased in plasma of patients with heart failure [5,6,7]. This is noteworthy in part because the

immunoassay system currently being used to measure BNP levels also detects proBNP, as the anti-BNP antibody cross-reacts with proBNP. Consequently, the present assay system actually measures not the active BNP level, but the total BNP (BNP+proBNP) level [8].

It is important to know the proBNP level and/or proBNP/total BNP ratio in heart failure, because proBNP has much less ability to induce cGMP production (about 13–17%) than BNP, and higher levels of the low-activity proBNP may be associated with the development of heart failure [7]. Consistent with that idea, we recently used the combination of gel-filtration and a fluorescent immunoenzyme assay with BNP extracted from plasma to show

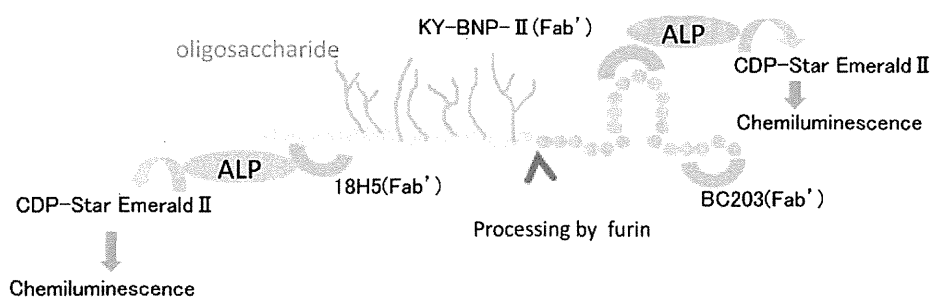


Figure 1. Schematic diagram of the total BNP and proBNP assay systems. BC203(Fab') is a common capture antibody in both systems. KY-BNP-II(Fab') is the detection antibody for the total BNP assay, and 18H5(Fab') is the detection antibody for the proBNP assay. ALP: Alkaline phosphatase; CDP-Star EmeraldII (Chemiluminescent Substrate): Disodium 2-chloro-5-(4-methoxy-spiro{1,2-dioxetane-3,2'-(5'-chloro)-tricyclo [3,3,1,13,7]decan}-4-yl)-1-phenyl phosphate.
doi:10.1371/journal.pone.0053233.g001

that although proBNP/total BNP ratios vary widely in heart failure, they are higher in cases of ventricular overload than in atrial overload [6]. Unfortunately, the method used in that study requires a great deal of time and effort, and extraction of the peptide from plasma may cause underestimation of the proBNP levels due to its high adsorptive property [9].

To overcome those shortcomings, we developed a sensitive method to more quickly and easily measure levels of proBNP and total BNP. Our idea was to make a sandwich immunoassay using a common capture antibody recognizing the C-terminal region of both BNP and proBNP and detection antibodies that recognize different epitopes: the N-terminal region of proBNP and the ring structure of BNP (Figure 1). Using this approach, we were able to develop a sensitive immunochemiluminescent assay for proBNP and total BNP in plasma. Here, we report on the assay's performance and its use to compare plasma levels of total BNP and proBNP in healthy subjects and patients with heart failure. In addition, we measured NT-proBNP and compared it with total BNP and proBNP.

Materials and Methods

All patients provided written informed consent for all blood sample analyses, and the protocol was approved by the Ethical Committee of Kyoto University Graduate School of Medicine. Sample analyses were also conducted in accordance with the policies and procedures of the Institutional Review Board for the use of human subjects in research at the Diagnostics Division of Shionogi & Co., Ltd.

Peptides and Reagents

Glycosylated proBNP and recombinant proBNP were purchased from Hytest Ltd. (Turk, Finland). The protein content was determined by amino acid analysis. BNP was from Peptide Institute, Inc. (Osaka, Japan). EZ-Link-sulfo-NHS-biotinylation kits were from Pierce (Rockford, IL). Sulfo-HMCS (N-(8-maleimidocapryloxy) sulfosuccinimide) was from Dojindo (Kumamoto, Japan). CDP/E (Disodium 2-chloro-5-(4-methoxy-spiro{1,2-dioxetane-3,2'-(5'-chloro)-tricyclo [3,3,1,13,7]decan}-4-yl)-1-phenyl phosphate) was from Applied Biosystems (Foster City, CA).

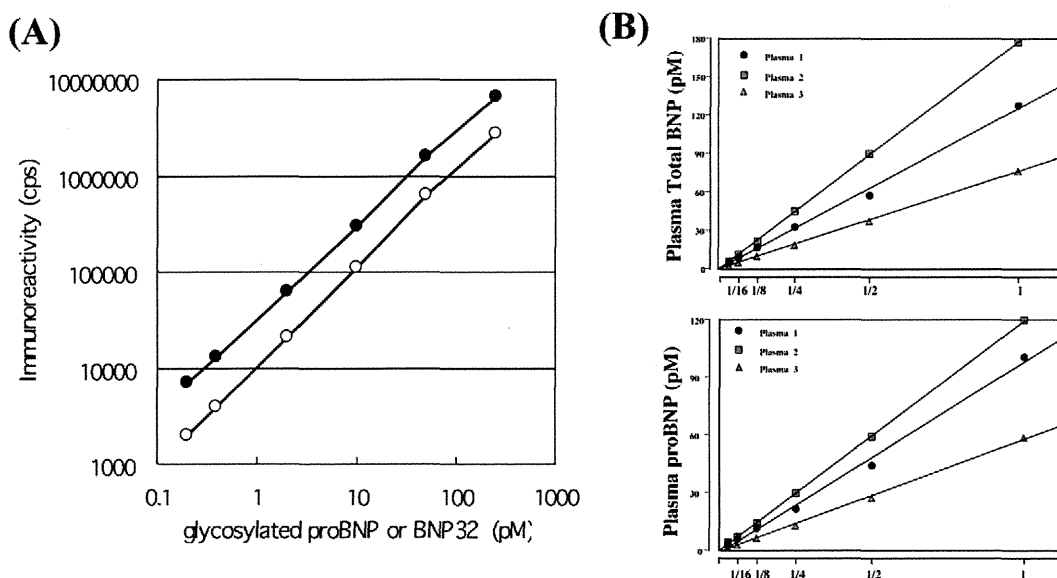


Figure 2. Standard curves for the proBNP (open circle) and total BNP (closed circle) assays (A). Plasma dilution curves (B). Three plasma samples collected from three heart failure patients were serially diluted with buffer.
doi:10.1371/journal.pone.0053233.g002

Table 1. Recovery of standard glycosylated proBNP and BNP added to human plasma.

Added peptide concentration, pmol/L	Recovery, %	
	proBNP assay system	total BNP assay system
2.0	90	85
25.0	101	97
100.0	95	95

doi:10.1371/journal.pone.0053233.t001

Antibodies

The monoclonal antibodies BC203 (IgG1, k) and KY-BNP-II (IgG1, k) were developed by Shionogi & Co., Ltd [10]. BC203 and KY-BNP-II recognize the C-terminal region and the ring region of BNP, respectively. The monoclonal antibody 18H5 was purchased from Hytest Ltd. 18H5 recognizes a region (a.a. 13–20) of proBNP. In the proBNP assay, the combination of BC203 (capture) and 18H5 (detection) was used because 18H5 is not affected by glycosylation [11]. In the total BNP assay, the combination of BC203 (capture) and KY-BNP-II (detection) was used because KY-BNP-II recognizes nearly all bioactive BNPs (Figure 1).

Preparation of BC203 coated immunoassay plates

BC203, which was the capture antibody in both assays, was biotinylated using an EZ-Link-sulfo-NHS-biotinylation kit according to the manufacturer's instructions. The biotinylated BC203 (0.2 mg/well in 100 mL PBS) was added to streptavidin-coated plates and incubated for 18 h at 4°C. After washing with a saline containing 0.01 g/dL Tween 20 and 0.05 g/dL sodium azide (Wash Buffer), the BC203 coated immunoassay plates were dried in a desiccator.

Preparation of 18H5 (Fab')-ALP and KY-BNP-II (Fab')-ALP

The 18H5 and KY-BNP-II mAbs (IgG) were digested with pepsin (IgG/pepsin = 1/0.05) for 4 h at 37°C in 100 mM citrate buffer (pH 4.0) containing 100 mM NaCl. Thereafter, Fab' solution was prepared by reduction with 10 mM 2-mercaptoethylamine in 0.1 M phosphate buffer (pH 6.0) containing 5 mM EDTA using the standard method [12]. Alkaline phosphatase from calf intestine (ALP; 2.0 mg or 14.2 nmol; Kikkoman, Chiba, Japan) in 0.475 mL 0.1 M Tris-HCl buffer (pH 7.0) containing 1 mM MgCl₂ and 0.1 mM ZnCl₂ was mixed with 31 mg (71 nmol) of Sulfo-HMCS in 0.05 mL of water for 1.5 h on ice,

after which the HMCS-activated ALP was purified on a PD-10 column (GE Healthcare, Chalfont St. Giles, UK). Aliquots of HMCS-activated ALP solution (0.96 mg in 0.192 mL) were each added to 0.441 mg of the Fab' in 0.15 mL of 0.1 M phosphate buffer (pH 6.0) containing 5 mM EDTA and mixed for 16 h at 4°C. Unlabeled Fab' antibody was removed using a TSKgel 3000SWxl column. The purified 18H5 (Fab')-ALP and KY-BNP-II (Fab')-ALP were then diluted with a StabilZyme AP (BioFX Lab.) and stored at 4°C until use.

Sandwich 2-step Chemiluminescent Enzyme Immunoassay

After the BC203 coated immunoassay plates were washed with a wash buffer, 50 mL of test sample or calibrator and 50 mL of Assay Buffer (0.05 M Tris-HCl buffer (pH 7.4), 1 g/dL BSA, 0.01 g/dL Tween80, 1 mM MgCl₂, 0.1 mM ZnCl₂, 1000K IU/mL Aprotinin, 0.1 mg/mL mouse gamma globulin, 0.9 g/dL NaCl) were added to the wells. The plates were then incubated for 3 h at 25°C. After washing with wash buffer, 100 mL of detection antibodies (18H5 (Fab')-ALP, 100 ng/ml; KY-BNP-II (Fab')-ALP, 416 ng/ml) were added to the wells. The plates were then incubated for 1 h at 25°C, followed by washing with wash buffer and addition of substrate (CDP/E) solution. The chemiluminescence from each well was then measured using a plate reader (Wallac 1420 Arvo sx, Perkin Elmer, Inc., MA).

Study Patients

We collected blood samples from heart failure patients (18 men and 14 women; age range, 34–84 years, mean age, 65±11 years) hospitalized at Kyoto University Hospital. The primary causes of the heart failure were ischemic heart disease (n = 8), cardiomyopathy (n = 8), valvular heart disease (n = 7), pulmonary hypertension (n = 7) and others (n = 2), which were diagnosed from the medical history, physical examination and chest radiographic, electrocar-

Table 2. Effects of dilution on recovery rates with the proBNP and total BNP assay systems.

Dilution magnitude	proBNP assay system		total BNP assay system	
	Measured, pmol/L	Recovery, %	Measured, pmol/L	Recovery, %
1	94	-	95	-
2	105	112	101	107
5	96	102	104	109
10	92	98	92	97
20	97	103	93	98
50	99	105	97	103
100	87	92	95	100

doi:10.1371/journal.pone.0053233.t002

Table 3. Intra- and Inter-assay precision of the proBNP assay systems.

	Added proBNP concentration pmol/L	Measured concentration pmol/L		CV %	Bias %
		Mean	S.D.		
Intra-assay (n = 5)	2.0	2.0	0.2	8.0	2.0
	25	25	1.3	5.2	0.0
	100	101	5.5	5.4	1.0
Inter-assay (n = 15)	2.0	1.9	0.1	5.3	-5.8
	25	23	1.7	7.4	-8.0
	100	96	6.1	6.4	-4.0

doi:10.1371/journal.pone.0053233.t003

diographic, echocardiographic and/or cardiac catheterization findings. Patients with symptomatic heart failure were under medication, including angiotensin-converting-enzyme inhibitors/angiotensin-receptor blockers, digitalis and diuretics. The New York Heart Association (NYHA) functional classes were class I–II (n = 19) and class III–IV (n = 13). Healthy subjects (61 men and 54 women; age range, 30–78 years, mean age, 50±10 years) were selected based on their normal physical, laboratory, chest radiographic, electrocardiographic and echocardiographic findings, and their BNP levels.

Plasma samples

Blood samples were drawn into plastic syringes and quickly transferred to chilled tubes containing EDTA (1.5 mg/mL, blood) and aprotinin (500 U/mL blood) and centrifuged at 1600× g for 20 min at 4°C. The obtained plasma samples were stored at -80°C until assayed.

Assay of plasma NT-proBNP levels

Plasma levels of NT-proBNP were measured using Elecsys proBNP II assay system (Roche Diagnostics, Basel, Switzerland).

Gel filtration chromatography

Plasma samples were extracted using Sep-Pak C18 cartridges (Waters, Milford, MA, USA) as previously described [6]. The eluate was lyophilized and dissolved in 30% acetonitrile containing 0.1% TFA. The resultant solution (300 ml) was separated by gel filtration HPLC on a Superdex 75 10/300 GL columns (10×300 mm×2, GE Healthcare) in the same buffer at a flow rate of 0.4 mL/min. The column effluent was fractionated every minute into polypropylene tubes containing bovine serum albumin

(100 mg) and each fraction was analyzed using the total BNP and proBNP assay systems. Because recent studies have shown that glycosylated proBNP with a MW of about 30 K circulates in the plasma [7], we examined the gel filtration positions at which commercial recombinant proBNP and glycosylated proBNP, and synthetic BNP were eluted to determine which is the major molecular form of BNP in human plasma.

Deglycosylation enzyme treatment

We further analyzed the immunoreactive proBNP levels to determine whether immunoreactive proBNP in plasma is glycosylated. Eluate lyophilized after extraction on a Sep-Pak C18 column was dissolved in phosphate buffer and incubated with or without a cocktail of deglycosylation enzymes for 24 h at 37°C, as previously described [13]. The enzyme cocktail included O-glycosidase (Roche Diagnostic) and neuraminidase (Roche Diagnostics) at final concentrations of 4.25 and 42.5 mU/mL, respectively. These two enzymes were essential for the deglycosylation, and the enzyme concentrations and incubation period were selected based on the results of preliminary and previously reported studies [11,13,14]. We then lyophilized the sample again and dissolved it in 30% acetonitrile containing 0.1% TFA, after which it was subjected to gel-filtration HPLC as described above.

Statistical Analysis

All values are expressed as means ± SD. The statistical significance of differences between 2 groups was evaluated using Fisher's exact test or unpaired Student's t test, as appropriate. Variables were compared among three groups using one-way analysis of variance followed by Bonferroni's multiple comparison

Table 4. Intra- and Inter-assay precision of the total BNP systems.

	Added BNP concentration pmol/L	Measured concentration pmol/L		CV %	Bias %
		Mean	S.D.		
Intra-assay (n = 5)	2.0	2.3	0.2	7.0	15.0
	25	25	2.1	8.4	1.0
	100	99	7.1	7.2	-0.7
Inter-assay (n = 15)	2.0	2.1	0.2	9.5	5.0
	25	24	1.7	2.9	-4.0
	100	100	1.9	1.9	0.0

doi:10.1371/journal.pone.0053233.t004

Table 5. Cross-reactivity between proBNP and BNP.

Added peptide concentration, pmol/L proBNP	Added peptide concentration, pmol/L BNP	Measured peptide concentration, pmol/L proBNP assay	Measured peptide concentration, pmol/L total BNP assay
50	50	58	114
100	10	113	119
10	100	8	113

doi:10.1371/journal.pone.0053233.t005

test. Correlation coefficients were calculated using linear regression analysis. Values of $P < 0.05$ were considered significant.

Results

Standard curve, recovery and precision

Figure 2 shows typical standard curves for the proBNP and total BNP assay systems. The lower detection limits were 0.04 pmol/L (proBNP) and 0.02 pmol/L (total BNP). At these levels the mean value ($n = 8$ each) of the chemiluminescence intensity (cps) was more than twice that at 0 pmol/L ($P < 0.05$). The working range (coefficient of variation (CV) $< 15\%$) of both assays was 0.2–250 pmol/L in total BNP and 0.4–250 pmol/L in proBNP, respectively.

Table 1 shows the recovery of standard proBNP and BNP, which was estimated from the levels of glycosylated proBNP or BNP added to clinically available plasma (endogenous total BNP = 0.3 pmol/L and proBNP = 0.2 pmol/L). In the proBNP assay system, using glycosylated proBNP as a standard, the recovery ranged from 90–101%. In the total BNP assay system, using BNP as the standard the recovery ranged from 85–97%. The effect of diluting plasma samples containing 100 pmol/L glycosylated proBNP or BNP is shown in Table 2. At every dilution level, the recovery rate was good. We also investigated the effects of dilution on plasma levels of total BNP and proBNP in three heart failure patients. As shown in Figure 2B, the calculated total BNP and proBNP values varied linearly with dilution (correlation coefficients = 0.998–1.00).

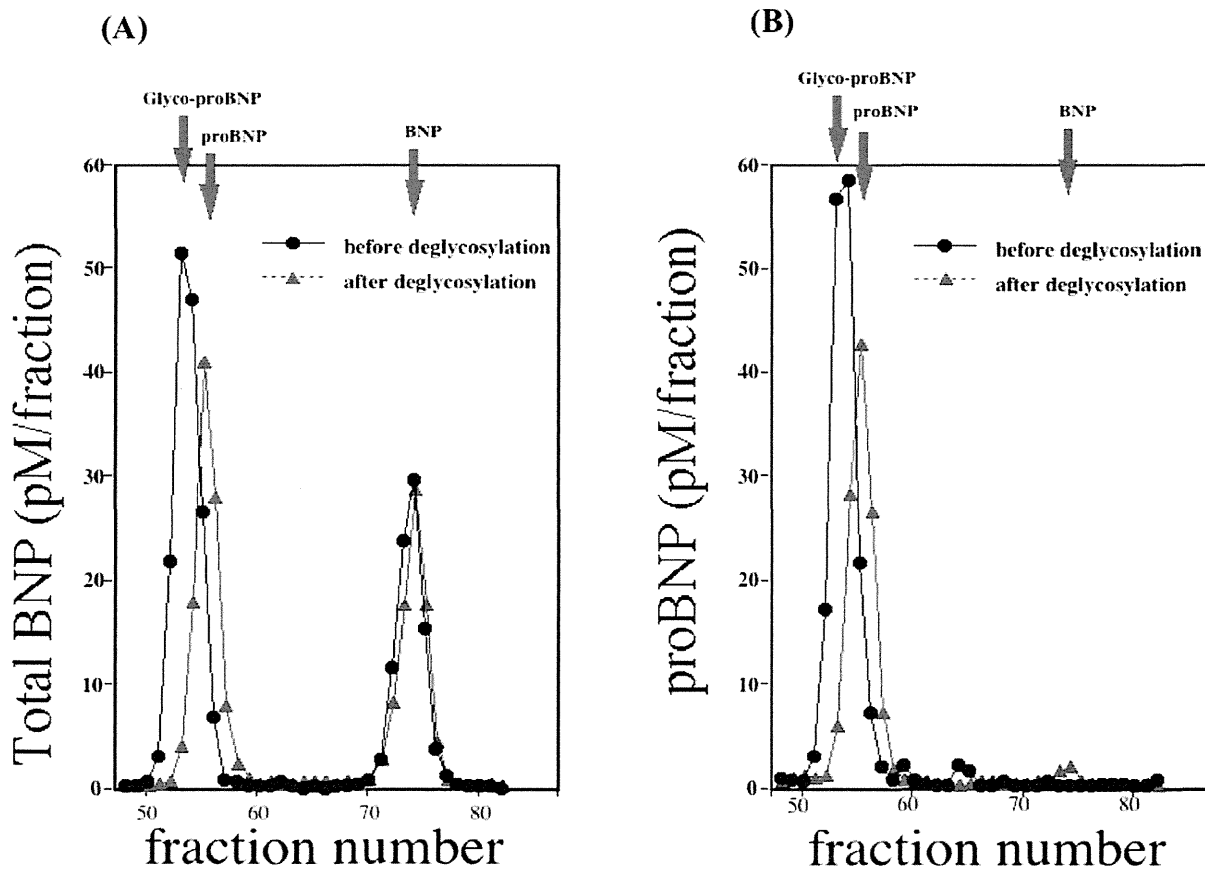


Figure 3. Gel filtration analysis of total BNP (A) and proBNP (B) in plasma from a heart failure patient. Fractions were assayed using the total BNP (A) and proBNP (B) systems. The elution points for glycosylated proBNP, proBNP and BNP are indicated by red arrows. Black and red lines respectively show gel filtration analyses of total BNP (A) and proBNP (B) in the same plasma sample before and after deglycosylation.
doi:10.1371/journal.pone.0053233.g003

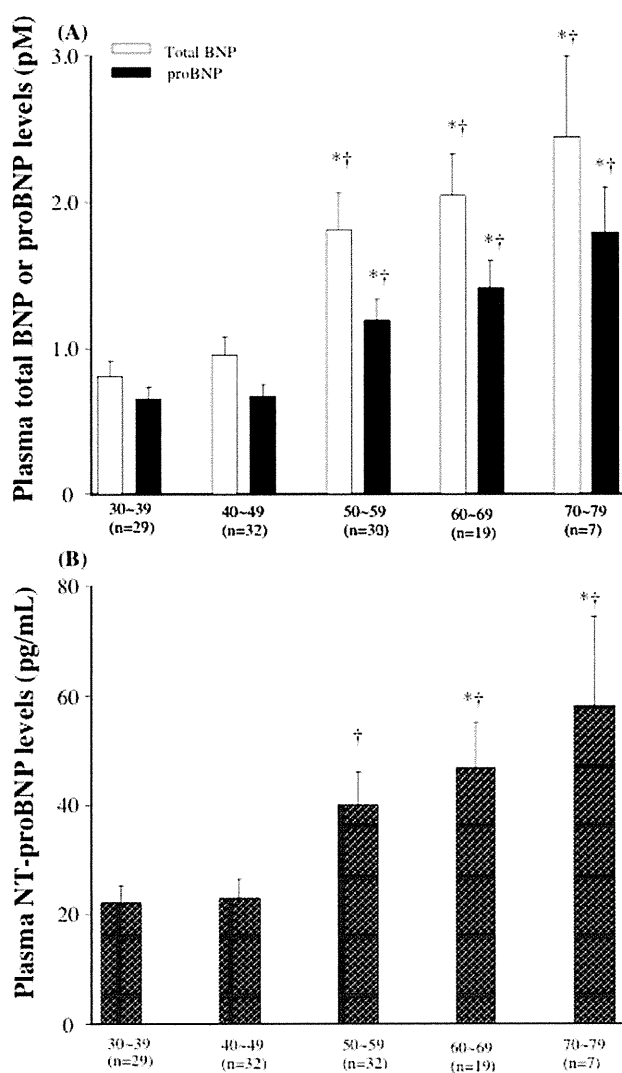


Figure 4. Plasma Levels of total BNP, proBNP, and NT-proBNP in different age groups. Bar graph showing the total BNP, proBNP (A) and NT-proBNP levels (B). Values are means \pm SE, * P <0.05 vs total BNP, proBNP, and NT-proBNP in 30~39, † P <0.05 vs total BNP, proBNP, and NT-proBNP in 40~49. doi:10.1371/journal.pone.0053233.g004

When we then assessed the intra- and inter-assay precision using plasma spiked with glycosylated proBNP or BNP, we found that the intra-assay CV ranged from 5.2%–8.0% in proBNP assay and from 7.0%–8.4% in total BNP assay, while inter-assay CV ranged from 5.3–7.4% in proBNP assay and from 1.9%–9.5% in total BNP assay, respectively (Table 3, 4).

Specificity and sensitivity

We next examined the cross-reactivity between proBNP and BNP. As shown in Table 5, the presence of BNP did not affect the values measured with the proBNP assay system. Moreover, the values measured with the total BNP assay system were the sum of the BNP and proBNP even at different compositions of these two peptides. Thus, the total BNP assay recognized both BNP and proBNP with the same efficiency and sensitivity. Likewise, the proBNP and total BNP assay systems recognized proBNP with the same efficiency and sensitivity.

Gel-filtration chromatography before and after deglycosylation procedure

Figure 3-A shows two immunoreactive BNP peaks detected using the total BNP assay with HPLC fractions. The first peak appeared in fractions 52–55 and the second peak in fractions 72–75. With the same sample, one immunoreactive BNP peak was detected by the proBNP assay (Figure 3-B); the position of that peak was completely consistent with the proBNP peak obtained with the total BNP assay. When subjected to gel filtration HPLC, recombinant proBNP, glycosylated proBNP and BNP were eluted mainly in fractions 53, 56 and 74, respectively. Treating the same plasma sample with an enzyme cocktail catalyzing deglycosylation shifted the first peak to fraction 54–56, which is consistent with the proBNP peak. From these results, we conclude that total BNP assay evaluates the sum of the glycosylated proBNP plus BNP, while proBNP assay detects glycosylated proBNP. The proBNP was not detected in a significant level with either assay system.

Plasma concentrations of proBNP, total BNP, and NT-proBNP in healthy subjects and heart failure patients

Plasma total BNP, proBNP and NT-proBNP levels in different age groups were shown in Figure 4-A, B. Plasma total BNP, proBNP and NT-proBNP levels appeared to increase according to the age. The older age groups (more than 50) had higher total BNP, proBNP and NT-proBNP levels than younger age groups (less than 50); however, there were no statistical differences in NT-proBNP between 30~39 and 50~59. In addition, there were significant positive relationships between plasma total BNP ($r = 0.467$, $p < 0.001$), proBNP ($r = 0.491$, $p < 0.001$) and NT-proBNP ($r = 0.376$, $p < 0.001$) levels and age (Figure 5-A, B, C).

The mean total BNP and proBNP in plasma from 116 healthy subjects were 1.4 ± 1.2 pM and 1.0 ± 0.7 pM, respectively (Figure 6-A). Female had higher total BNP than male (total BNP: 1.7 ± 1.3 vs 1.1 ± 1.1 , $P < 0.05$; proBNP: 1.1 ± 0.8 vs 0.8 ± 0.6 pM, $P = 0.11$) (Figure 6-C). proBNP/total BNP ratio was lower in female than that in male. NT-proBNP was also higher in female than those in male (Figure 6-E). The total BNP and proBNP levels were markedly elevated in heart failure patients, and the magnitude of the increase reflected the severity of the patients' condition as observed in NT-proBNP (Figure 6-A, B).

Discussion

Plasma levels of the cardiac hormone BNP increase in proportion to the severity of heart failure. Indeed, plasma BNP levels are used as a biomarker of heart failure, and the guidelines in many countries recommend that BNP be used as a diagnostic indicator of acute and chronic heart failure [1–3]. The stimuli that increase cardiac BNP production include pressure overload, volume overload and ischemia, as well as various cytokines and neurohumoral factors [15]. In response to these stimuli, BNP mRNA expression is rapidly upregulated. Following translation of the protein, the signal peptide is removed to produce proBNP, which is then cleaved into BNP and the NT-proBNP fragment during secretion [15]. It is noteworthy that BNP and proBNP could not be distinguished from one another in earlier BNP assay systems because the anti-BNP antibodies cross-reacted with proBNP. We therefore endeavored to develop a new assay system that would enable separate measurement of BNP and proBNP. Recent studies have shown that levels of uncleaved proBNP are increased in heart failure to a greater degree than BNP [5–7,16]. Using a combination of gel filtration and an immunoenzyme fluorescent assay for BNP, we previously found that proBNP levels are increased in heart failure and that the proBNP/total BNP

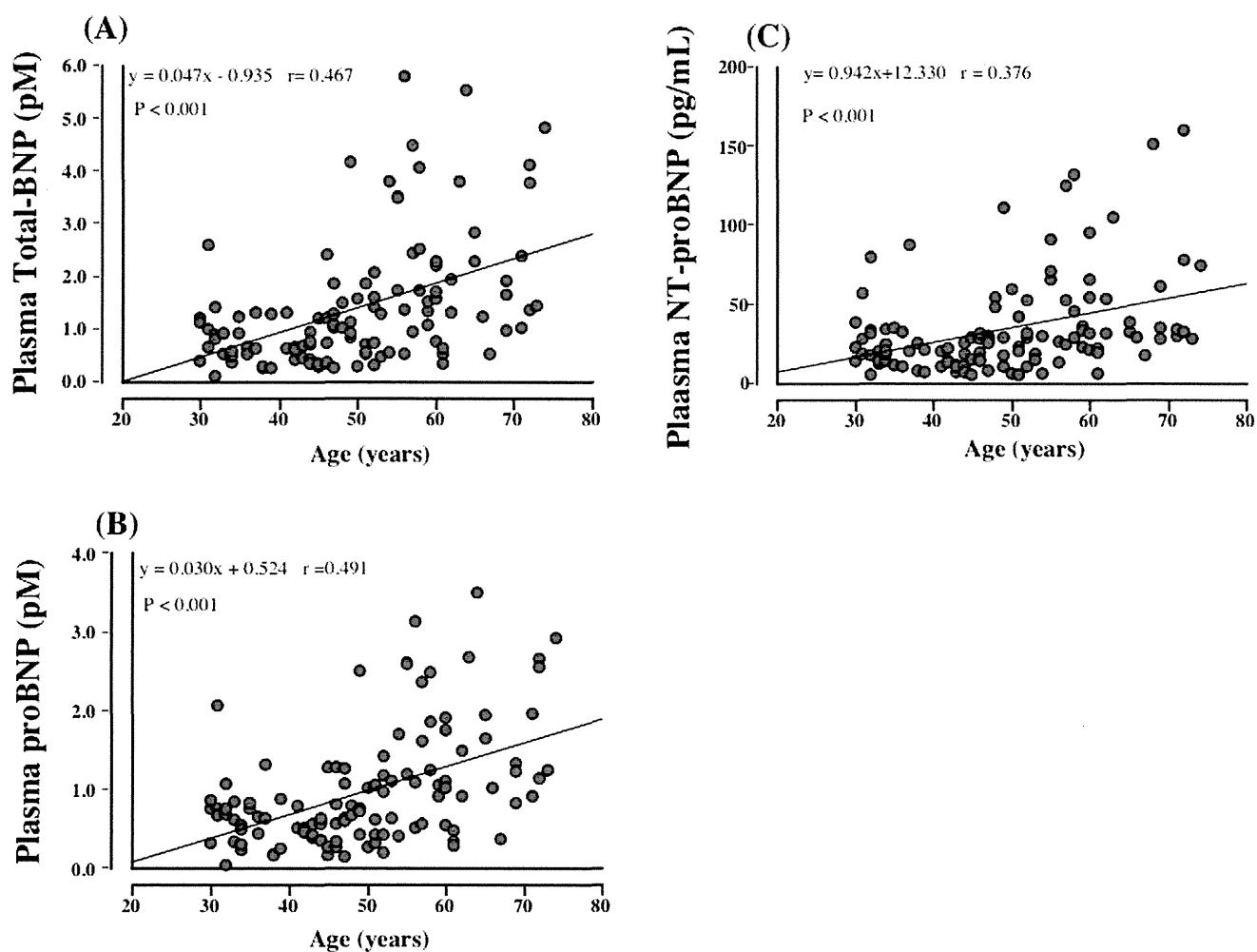


Figure 5. The relationships between total BNP (A), proBNP (B), and NT-proBNP (C) and age.
doi:10.1371/journal.pone.0053233.g005

ratios are higher in heart failure patients with ventricular overload than those with atrial overload [6]. Although this protocol provides useful information, the methodology is time-consuming and impractical for routine assays in clinical laboratories. In addition, recovery of proBNP may be diminished by both extraction and the gel filtration steps [9,16]. To overcome these problems, we developed new direct immunochemiluminescent assays for proBNP and total BNP.

We used two monoclonal antibodies, BC203 and 18H5, to assay proBNP. BC203 recognizes an epitope in the C-terminal of proBNP, while 18H5 recognizes an epitope in the N-terminal. Recent studies showed that proBNP has seven sites suitable for *O*-linked oligosaccharide attachment (Ser36, Thr37, Thr44, Thr48, Thr53, Ser58 and Thr71) within the N-terminal portion of the peptide [14]. Because the *O*-linked oligosaccharide attachments almost completely inhibit the binding of the antibody to the peptide [17], we selected 18H5, which recognizes the N-terminal of proBNP (a.a. 13–20) in a region not subject to glycosylation (Figure 1). To assay total BNP, we used the monoclonal antibodies BC203 and KY-BNP-II, as previously reported [10]. In both assays, BC203 served as the capture antibody. Importantly, because the affinity of 18H5 for the N-terminal portion is similar to the affinity of KY-BNP-II for the ring structure, we are able to calculate the proBNP/total BNP ratio. In addition, our new assays

are less time-consuming and more sensitive and accurate than earlier ones, and the lower detection limits for total BNP (0.02 pmol/L) and proBNP (0.04 pmol/L) enabled us to measure plasma proBNP levels in nearly all the healthy subjects tested.

We used gel-filtration on two tandemly connected Superdex 75 columns to determine the molecular mass of plasma proBNP. As shown in Figure 3-A,B, a single peak of proBNP was obtained in both the total BNP and proBNP assay systems. The elution points are consistent with that of glycosylated proBNP, but not deglycosylated proBNP, and deglycosylation treatment significantly shifted the peak rightward (Figure 3-A,B) to an elution point consistent with proBNP. The peak immunoreactivity of proBNP after deglycosylation was slightly smaller than before treatment, suggesting the recovery rate of proBNP after gel-filtration is lower than that of glycosylated proBNP, which is consistent with proBNP being more adsorptive than glycosylated proBNP. Our findings are also consistent with previous Western blot analyses showing that plasma levels of glycosylated proBNP are elevated and no substantial level of proBNP is detected in severe heart failure [7]. Taken together, these results suggest that the major molecular form of proBNP in the plasma of patients with heart failure is the glycosylated form.

ProBNP is also the important molecular form of BNP in the plasma of healthy subjects. When we previously used gel-filtration